공학석사 학위논문

# A Stochastic Progressive Damage Simulation Model for Fiber Reinforced Polymer Laminates

## 섬유강화 폴리머 적층 복합재료의 확률론적 점진 손상해석 모델

2019 년 2 월

서울대학교 대학원

기계항공공학부

정승우

# A Stochastic Progressive Damage Simulation Model for Fiber Reinforced Polymer Laminates

## 섬유강화 폴리머 적층 복합재료의 확률론적 점진 손상해석 모델

지도 교수 윤 군 진

이 논문을 공학석사 학위논문으로 제출함
2018 년 11 월

서울대학교 대학원
기계항공공학부
정 승 우

정승우의 공학석사 학위논문을 인준함
2018 년 12 월

위 원 장 김 규 홍 (인)

부위원장 윤 군 진 (인)

위 원 신 상 준 (인)

## Abstract

# A Stochastic Progressive Damage Simulation Model for Fiber Reinforced Polymer Laminate

Sungwoo Jeong
Department of Mechanical and Aerospace Engineering
The Graduate School
Seoul National University

Fiber reinforced polymer matrix composites (FRPMC) laminate composites are widely used for its high strength and high stiffness-to-weight ratio. Although FRPMC holds many advantages, it has low matrix strength. This thesis proposes a stochastic progressive damage simulation model for FRPMC laminates. Damage mechanisms considered in this thesis are internal damages of fiber and matrix. Deterministic predictions by the existing damage progressive analysis model of laminate composites could be very different from the experimental global strength and failure modes due to effects of material uncertainties. In polymer matrix composites, such material

uncertainties arise from different cure kinetics and chemically induced shrinkage. Therefore, uncertainties of constituents' physical properties were taken into account in this study. An anisotropic damage model was used for damage initiation and evolution of each layer. Strength and fracture energy of layers were modelled as spatially varying random fields through the Karhunen–Loeve expansion method. For demonstrations of the proposed stochastic progressive damage analysis, a three–dimensional meso–scale finite element model of a multiple–layer was developed.

Keywords : Stochastic simulation, progressive damage simulation, fiber–reinforced polymer matrix composites, strength, fracture energy

Student Number : 2017–25727

# Table of contents

# List of figures

# List of tables

# 1. Introduction

## 1.1. Background and Motivation

Fiber reinforced polymer matrix composites are being widely used in advanced structure components in aerospace, automotive, sports, and many other industries due to their outstanding properties such as lightweight, high strength and high stiffness. However, composite materials have a weak point in the transverse direction due to low strength of the matrix.

Continuum damage mechanics (CDM) model has a long history of developments and applications to laminate composite materials. Damage parameters were adopted instead of physical lamina damage. Early work on CDM models for laminate composite was focused on damage variable and its uses for stiffness degradation [1]. Ladeveze [2] proposed the damage state caused by only the shear and transverse moduli. Talreja proposed a damage related vector that represents microcrack density on various planes[3, 4]. In the meantime, Lene proposed a method for modeling fiber/matrix debonding using a scalar damage variable [5]. In those early works,

damage evolution was not highlighted. For modeling of the damage evolution, there are two different approaches: 1) empirical approach and 2) a formulation using free energy function.

Allen and his coworkers proposed a CDM model that incorporates a set of second-order tensor-valued internal state variables representing locally averaged measures of specific damage states such as matrix cracking, fiber-matrix debonding, and interlaminar cracking [6, 7]. Damage material constitutive equations were formulated with thermodynamic constraints imposed on the internal state variables at the local scale. From these results, they expanded the Helmholtz free energy in terms of strain, temperature and the internal state variables for the CDM model [6, 7].

On the other hand, Barbero and his coworkers also proposed a similar approach for CDM modeling coupled with the classical plasticity model within a consistent thermodynamic framework using internal state variables [8]. They also suggested a novel implementation method into finite element formulation considering geometrical nonlinearity. Their model was extended to include triaxial orthotropic damage in terms of three damage eigenvalues

[9]. Their models have advantages of simplicity and generality in implementation and extensibility, respectively.

Voyiadjis and his coworkers coupled damage progression and plasticity using a symmetric second-order damage tensor[10-12]. Eigenvectors of the damage tensor are interpreted as the principal direction of the damage and its corresponding eigenvalues have physical meaning of damage density in the normal direction to the eigenvectors. In their models, the damage was counted for each constituent, that is, fiber and matrix and homogenization was performed on the damaged microstructure.

Lapczyk [13] implemented an orthotropic damage model of brittle fiber reinforced materials. In his model, crack band model was implemented to alleviate the mesh dependency of the solution. Commercial software use his model for fiber reinforced damage analysis. However, this model is only for two-dimensional material. Demands of three-dimensional orthotropic material model still increase.

The manufacturing of composites consists of process that is difficult to control. Uncertainty in a manufactural process can cause

variabilities in material properties. Many researches have studied stochastic damage analyses for the reliability of laminate composites [14−20]. Chiachio et al.[21] reviewed reliability in composites. Most of researches considered material properties as random variables. Only few research handled material properties as spatial random fields: low velocity impact[17] and weakest link theory [22]. Further study on the 3D progressive damage analysis with material random field is still on demand.

## 1.2. Objectives and Thesis Overview

Objectives of this thesis are to implement stochastic progressive damage analysis (PDA) algorithm for three−dimensional FRPMC materials and investigate effects of stochastic variations of material properties on the PDA results. This thesis is organized as follow :

Section 0 describes the material model based on CDM. Hashin damage failure criterion was adopted. The damage evolution was based on fracture energy. Numerical implementation was presented including a viscous regularization technique. A stochastic progressive damage analysis code was implemented with ABAQUS user defined

subroutine UMAT. Verification of UMAT code was carried out using a thin single layer FE model with built-in damage material constitutive model.

Section 2 illustrates random field modeling technique for spatial distributions of material properties considering the fiber orientation. A continuous covariance kernel was discretized by the Galerkin finite element approach. The covariance kernel was modified in order to account for effects of fiber orientation.

Section 0 includes a numerical example for stochastic progressive damage analysis of FRPMC. Six different strengths and fracture energy were assumed as spatial random fields. Discussions on the results were included. Finally, conclusions and future works were described in Section 4.4.

## 2. Spatial randomness of material properties

Compared to ordinary materials, composites have difficulties in manufacturing with a uniform distribution of fiber. FRPMC laminate varied significantly by the amount of resins in each ply. Matrix also has defects such as voids. Spatial material distribution was

considered due to these reasons. Derivation of equations in this chapter is based on previous research of the author[23].

## 2.1. Modeling of three-dimensional random field of materials.

For the sake of modeling spatially distributed materials, this paper adopted three-dimensional Karhunen-Loeve Expansion (KLE). A typical ramdom field consists of two parts: the deterministic part and the stochastic part with a series expansion.

The KLE decomposes a random field T is represented as following Eq. (1)

$$T(\vec{P}) = \langle T(\vec{P}) \rangle + \sum_{i=1}^{\infty} \sqrt{\lambda_i}\, \phi_i(\vec{P})[\xi_i(\omega)] \qquad \textbf{(1)}$$

In this equation, $\vec{P}$ is position vector; angled bracket < > represents mean value of variable; $\lambda_i, \phi_i$ are eigenvalues and eigenfunctions respectively; $\xi_i$ is random variable which can follow statistical distribution; $\omega$ is the primitive randomness; and the bracket [ ] represents randomly sampled set of variable. Eigenvalues and eigenfunctions are solution of following Fredholm integral

equation with analytical covariance kernel.

$$\int_{\Omega_Q} C(\vec{P},\vec{Q})\,\phi_i(\vec{Q})dV_Q = \lambda_i\phi_i(\vec{P}) \quad \textbf{(2)}$$

$$C(\vec{P},\vec{Q}) = \sigma^2\exp\left(-\frac{\lfloor x_P - x_Q \rfloor}{L_x} - \frac{\lfloor y_P - y_Q \rfloor}{L_y} - \frac{\lfloor z_P - z_Q \rfloor}{L_z}\right), \vec{P},\vec{Q} \in \Omega \quad \textbf{(3)}$$

Where $dV_N = dx_N dy_N dz_N$ is the volume related to position vector N (N=P, Q); $\sigma$ is the standard deviation; $x_N, y_N, z_N$ are coordinate of position vector N (N=P, Q); and $L_i$ is correlation length in i−th direction. Fiber reinforced polymer have orthotropic material behavior. In order to consider orthotropic correlation, different correlation length for each direction was adopted in this thesis.

## 2.2. Numerical implementation of KL expansion

To apply material randomness into finite element structural analysis, the Galerkin finite element approach is adopted to solve Eq. (2). Lagrangian interpolation function was used to eigenfunctions as follow

$$\phi_{\mathrm{i}}(\vec{Q}) = \mathrm{N}(\vec{Q})\mathrm{d_e} \tag{4}$$

Where $\mathrm{N}(\vec{Q})$ and $\mathrm{d_e}$ are matrix form of interpolation function and eigenfunctions respectively. With residual integration, Eq. (2) is derived as follow

$$\left[\int_{\Omega_\mathrm{P}}\int_{\Omega_Q} C(\vec{P},\vec{Q})\,\mathrm{N}(\vec{P})^{\mathrm{T}}\mathrm{N}(\vec{Q})|\mathrm{J}_e|^2 dV_Q dV_P\right]\mathrm{d_e} = \lambda_i\left[\int_{\Omega_\mathrm{P}}\mathrm{N}(\vec{P})^{\mathrm{T}}\mathrm{N}(\vec{Q})|\mathrm{J}_e|dV_P\right]\mathrm{d_e} \tag{5}$$

In the above equation, $|\mathrm{J}_e|$ is the determinant of Jacobian matrix for mapping from isoparametric coordinate to physical coordinate. Eq. (5) represents single elemental relation. By assembling all elements, global eigenvalue equation is derived as follow

$$\sum_{E_P=1}^{NE_{RF}}\sum_{E_Q=1}^{NE_{RF}}\left[\int_{\Omega_\mathrm{P}}\int_{\Omega_Q} C(\vec{P},\vec{Q})\,\mathrm{N}(\vec{P})^{\mathrm{T}}\mathrm{N}(\vec{Q})|\mathrm{J}_e|^2 dV_Q dV_P\right]\mathrm{D} = \delta_{\mathrm{ij}}\lambda_i\sum_{E_P=1}^{NE_{RF}}\left[\int_{\Omega_\mathrm{P}}\mathrm{N}(\vec{P})^{\mathrm{T}}\mathrm{N}(\vec{Q})|\mathrm{J}_e|dV_P\right]\mathrm{D} \tag{6}$$

Here, $NE_{RF}$ denotes number of random field elements. Eq. (6) is rewritten as follow

$$\mathrm{BD} = \Lambda \mathrm{MD} \tag{7}$$

Where,

$$\mathrm{B} = \sum_{E_P=1}^{NE_{RF}} \sum_{E_Q=1}^{NE_{RF}} \left[ \int_{\Omega_P} \int_{\Omega_Q} C(\vec{P}, \vec{Q})\, \mathrm{N}(\vec{P})^{\mathrm{T}} \mathrm{N}(\vec{Q}) |\mathrm{J}_e|^2 dV_Q dV_P \right] \tag{8}$$

$$\mathrm{M} = \sum_{E_P=1}^{NE_{RF}} \left[ \int_{\Omega_P} \mathrm{N}(\vec{P})^{\mathrm{T}} \mathrm{N}(\vec{Q}) |\mathrm{J}_e| dV_P \right] \tag{9}$$

$$\Lambda = \delta_{\mathrm{ij}} \lambda_i \tag{10}$$

By applying finite element, the FE based KLE random fiels is expressed as follow

$$T(\vec{P}) = \ < T(\vec{P}) > \ + \sum_{i=1}^{m} \sqrt{\lambda_i}\, \phi_i(\vec{P}) [\xi_i(\omega)] \tag{11}$$

In the above equation, m is number of eigenfunctions to consider. In this thesis, second order finite element is used to construct B matrix because of high accuracy.

Figure 2.1 shows the reduced eigenvalues with respect to increasing modes. The first several eigenvalues are more significant among the entire modes.

Eigen modes are truncated for computational efficiency with being 95% in entire summation of eigenvalues.

Figure 2.2 shows the first three eigenfunctions in the 3D domain($\Omega$) with different correlation length in x direction. . Figure 2.3 illustrates the effect of correlation length and standard deviation on random field variable. As the $L_z$ increases, the fluctuation of the random field in z direction decreases. As $\sigma$ increases, the increasing depth of the fluctuation can be observed.

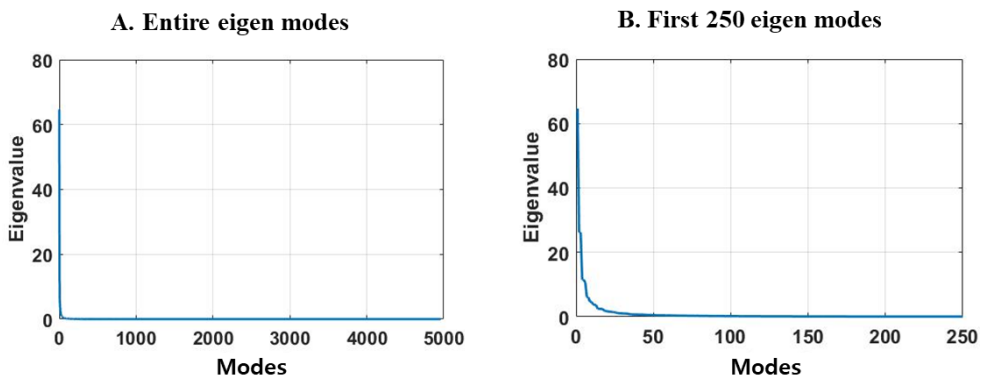


**Figure 2.1 a plot of decreasing eigenvalue**

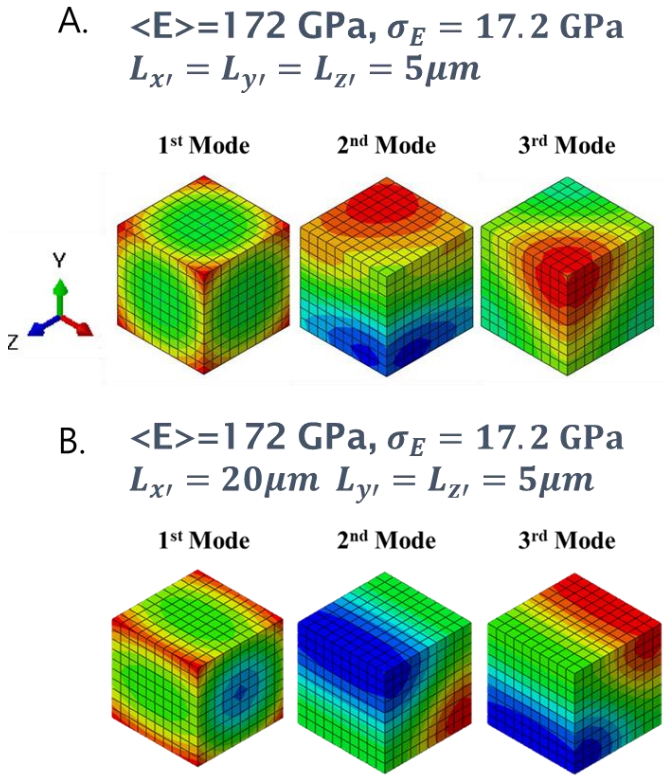


**Figure 2.2 First three modes of eigenfunctions with different correlation length**

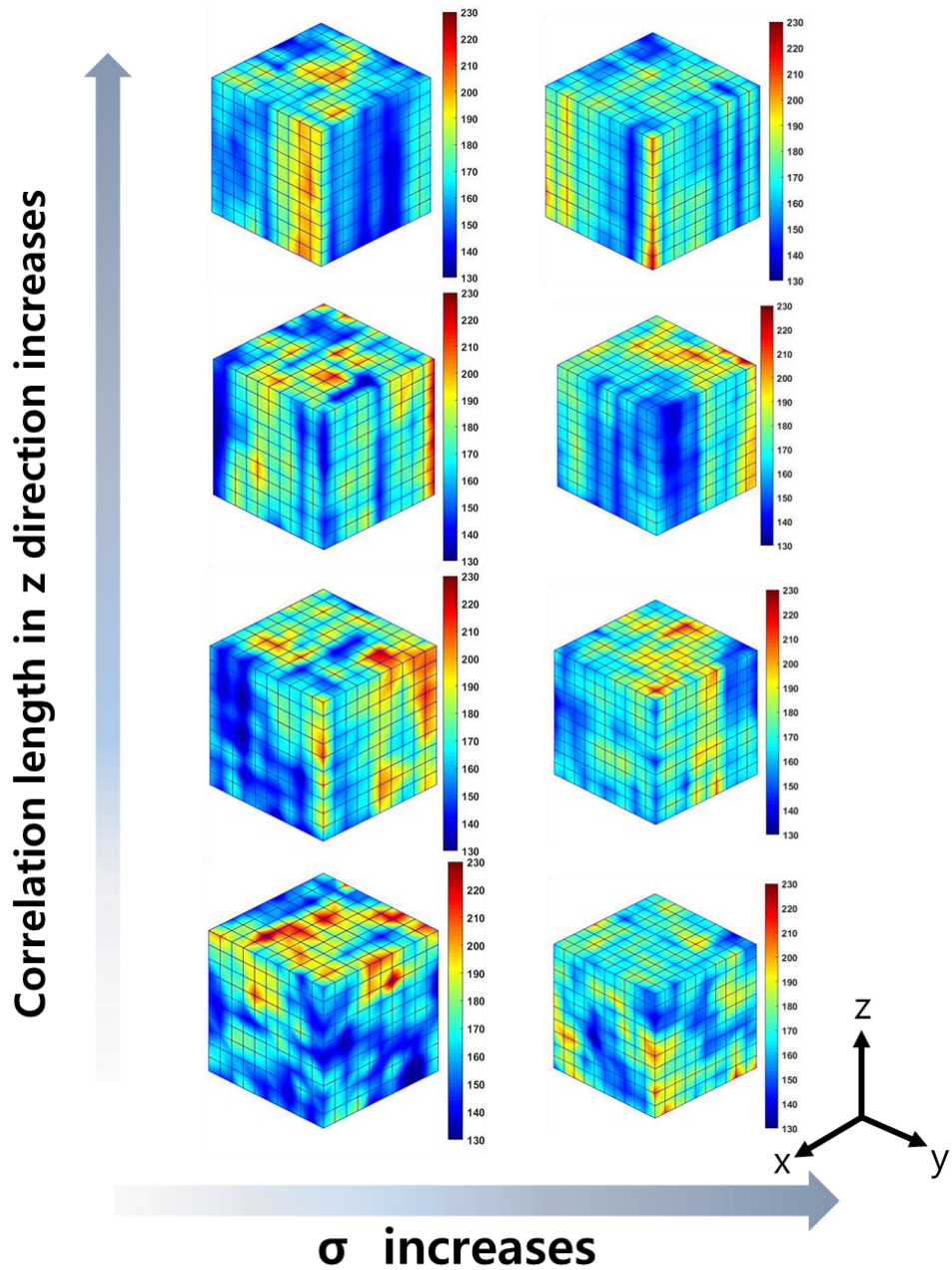


**Figure 2.3 Effects of standard deviation and correlation length in one direction of random fields in 3D space**

## 2.3. Application for fiber reinforced polymer

Laminate composites are made of layer which have different fiber orientation such as 0°, 45° and 90°. For the sake of considering fiber orientation, rotational tensor was adopted. Coordinate system based on fiber direction have a relation with global coordinate system

$$[\mathrm{R}] = \begin{bmatrix} \frac{\partial x'}{\partial x} & \frac{\partial x'}{\partial y} & \frac{\partial x'}{\partial z} \\ \frac{\partial y'}{\partial x} & \frac{\partial y'}{\partial y} & \frac{\partial y'}{\partial z} \\ \frac{\partial z'}{\partial x} & \frac{\partial z'}{\partial y} & \frac{\partial z'}{\partial z} \end{bmatrix} \tag{12}$$

$$\{x'\} = [R]\{x\} \tag{13}$$

The relation between both coordinate system with rotational angle was shown in Figure 2.4. Z' axis of material coordinate system aligns in XY plane of a global coordinate system.

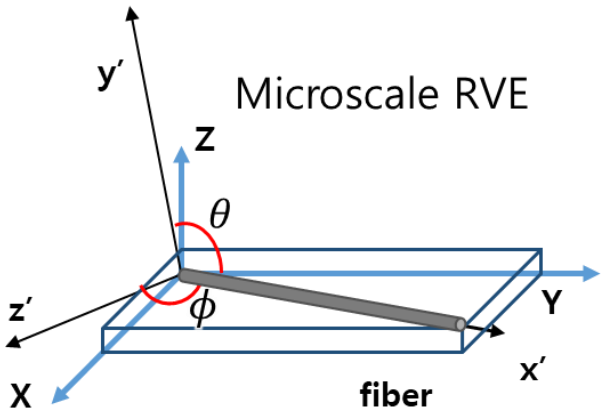


**Figure 2.4 Material coordinate system with fiber orientation**

Using the angle between two coordinate system, rotational tensor with angle can be expressed as

$$[\mathrm{R}] = \begin{bmatrix} sin\theta cos\phi & -cos\theta cos\phi & sin\phi \\ sin\theta sin\phi & -cos\theta sin\phi & -cos\phi \\ cos\theta & sin\theta & 0 \end{bmatrix} \quad \textbf{(14)}$$

Covariance kernel was modified with material coordinate system as follow

$$C(\vec{\boldsymbol{P}}, \vec{\mathbf{Q}}) = \sigma^2 \exp\left( -\frac{\left|x'_{\mathbf{P}} - x'_{\mathbf{Q}}\right|}{L_x} - \frac{\left|y'_{\mathbf{P}} - y'_{\mathbf{Q}}\right|}{L_y} - \frac{\left|z'_{\mathbf{P}} - z'_{\mathbf{Q}}\right|}{L_z} \right), \vec{\boldsymbol{P}}, \vec{\mathbf{Q}} \in \Omega \quad \textbf{(15)}$$

Here, the KLE can be expressed using different coordinate system. Figure 2.5 illustrates material spatial distribution with three different aligns of a fiber (45°, 90° and 0°).

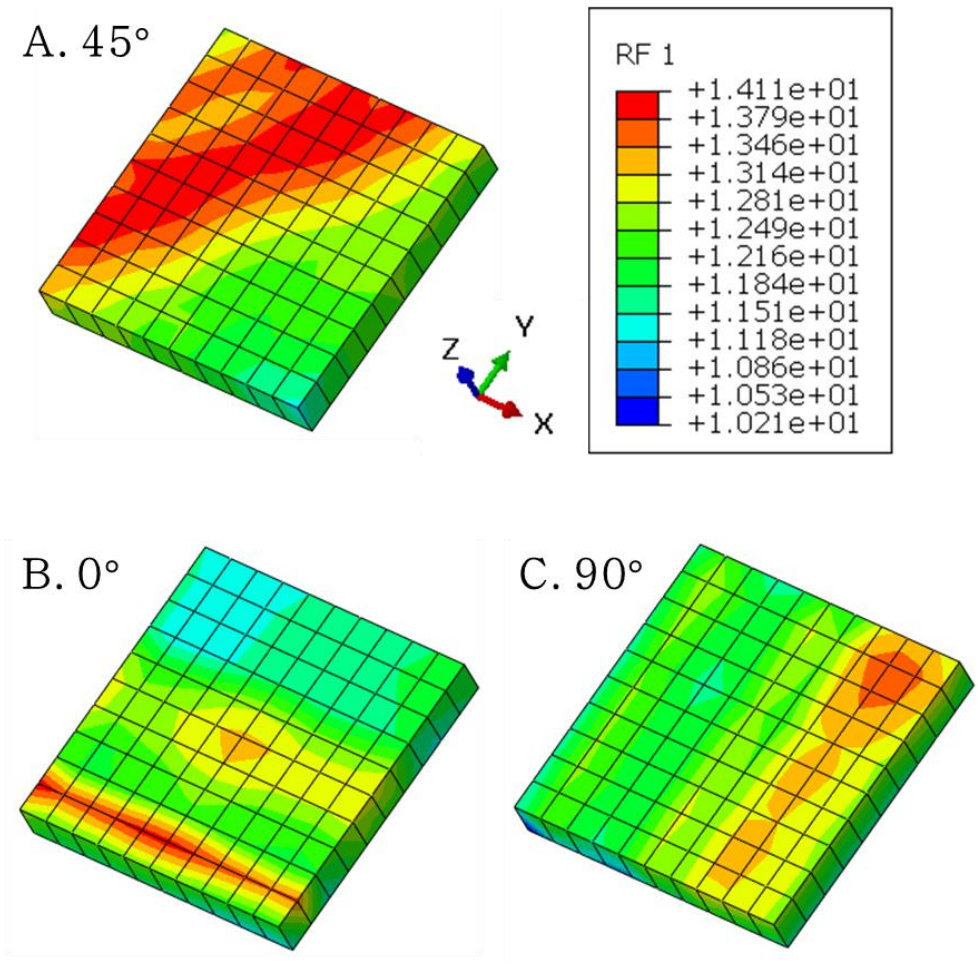


Figure 2.5. Spatial material properties with different orientation angle of a fiber (A) 45°, (B) 0° and (C) 90°

# 3. Progressive damage analysis model of fiber-reinforced polymer matrix composites

Unidirectional lamina is considered as orthotropic material. If fiber aligned in x−axis, material has symmetric characteristics such as $\mathrm{E_y} = E_z, \nu_{xy} = \nu_{xz}$ and $G_{xy} = G_{xz}$.

Carbon fiber reinforced polymer matrix composites usually exhibit elastic−brittle behavior as observed in many literatures such as Matzenmiller et al.[24]. Plastic deformation is not significant in the elastic−brittle material. Consequently, elastic material behavior is assumed.

Progressive damage analysis is already adopted in the commercial software; ABAQUS. However, progressive damage analysis in ABAQUS is limited only to two−dimensional element. In this thesis, three−dimensional progressive damage model was implemented in ABAQUS user−subroutine for material (UMAT).

## 3.1. Damage initiation criteria

Failure criterion is generally used for the prediction of the damage initiation. The damage initiation is followed by softening

behavior. In this thesis, Hashin's failure criterion [25] was selected whereby criteria for both compression and tension states of matrix and fiber are defined. Hashin's failure criteria equations are represented as follows

$$e_{ft} = \left(\frac{\sigma_{11}}{F_{1t}}\right)^2 + \alpha\left(\frac{\sigma_{12}+\sigma_{13}}{F_{ls}}\right)^2 \geq 1 \tag{16}$$

$$e_{fc} = \left(\frac{-\sigma_{11}}{F_{1c}}\right)^2 \geq 1 \tag{17}$$

$$e_{myt} = \left(\frac{\sigma_{22}}{F_{2t}}\right)^2 + \left(\frac{\sigma_{12}}{F_{ls}}\right)^2 + \left(\frac{\sigma_{23}}{F_{ts}}\right)^2 \geq 1 \tag{18}$$

$$e_{myc} = \frac{1}{4}\left(\frac{-\sigma_{22}}{F_{ls}}\right)^2 + \left(\frac{F_{2c}^2}{4F_{ls}^2} - 1\right)\frac{\sigma_{22}}{F_{2c}} + \left(\frac{\sigma_{12}}{F_{ts}}\right)^2 \geq 1 \tag{19}$$

where $e_m$ (m=ft,fc,mt,mc) is the material state related to the damage state; $F_{1t}, F_{1c}, F_{2t}, F_{2c}, F_{ls}, F_{ts}$ are axial tensile strength, axial compressive strength, transverse tensile strength, transverse compressive strength, longitudinal shear strength and transverse shear strength, respectively; and $\alpha$ is the coefficient to consider shear effects on the axial damage. This coefficient was taken as 1 by Hou [26] and Hashin [25]. It was considered as 0 by Guo [27]. In this thesis, the coefficient $\alpha = 0.06$ is adopted following literature

Chao [28]. Eq. (18) and (19) were based on Davila and Camanho model [29]. Delamination is damage related to inter−lamina damage. In this mode, delamination is not considered.

## 3.2. Damage evolution process

Material stiffness is degraded with damage variable after failure was initiated. The crack band model with a characteristic element length was implemented by Lapczky et al. [13]. The dissipated energy of elements can be written as follow

$$G_I = \frac{1}{2}\sigma_{I,eq}^{o}\varepsilon_{I,eq}^{o}l_c \tag{20}$$

In this equation $G_I$ is the dissipated energy of each mode; $\sigma_{I,eq}^{o}$ and $\varepsilon_{I,eq}^{o}$ are the equivalent stress and strain when the damage is initiated; subscript I represents each four damage mode (I=ft, fc, mt, mc); superscript o depicts the damage onset; and $\boldsymbol{l_c}$ is the characteristic length. A typical characteristic length of a first order element is a line across the element.

The evolution of damage variable of each mode $\mathbf{d_I}$ is expressed as follows.

$$d_I = \frac{\delta_{I,eq}^f(\delta_{I,eq} - \delta_{I,eq}^o)}{\delta_{I,eq}(\delta_{I,eq}^f - \delta_{I,eq}^o)}, \qquad \delta_{I,eq}^o \le \delta_{I,eq} \le \delta_{I,eq}^f \tag{21}$$

where $\delta_{I,eq}^f$ is the equivalent displacement; and the superscript 'f' means the fully damaged state. Equivalent stress and displacement were calculated as summarized in Table 3.1. The damage variable has a value between 0 and 1. $\delta_{I,eq}^o$ is calculated using equations in Table 3.1.

Fully damaged equivalent displacement was assumed as follows

$$\delta_{I,eq}^f = \frac{2G_I}{\sigma_{I,eq}^o} \tag{22}$$

In Eq. (22), $\sigma_{I,eq}^o$ is the equivalent stress when the damage onset is calculated as Table 3.1. The relation of Eq. (22) was depicted in Figure 3.1. The fracture energy $\mathrm{G_I}$ plays an important role in predicting the ultimate failure. Maimi et al. [30] studied how the fracture energy is obtained using the tests. However, it is not always easy to measure the fracture energy by experiments. Generally, the fracture energy was assumed for the sake of the numerical computation [13].

**Table 3.1 Equivalent displacement and stress with characteristic length**

| Failure modes | Equivalence displacement | Equivalence stress |
|---|---|---|
| Fiber tension | $\delta_{ft,eq} = L_C\sqrt{< \varepsilon_{11} >^2 + \alpha(\varepsilon_{12}^2 + \varepsilon_1^2}$ | $\sigma_{ft,eq} = \frac{L_C(< \sigma_{11} >< \varepsilon_{11} > + \alpha\sigma_{12}\varepsilon_{12} + \alpha\sigma_{12}}{\delta_{ft,eq}}$ |
| Fiber compression | $\delta_{fc,eq} = L_C < -\varepsilon_{11} >$ | $\sigma_{fc,eq} = \frac{L_C(< -\sigma_{11} >< -\varepsilon_{11} >)}{\delta_{fc,eq}}$ |
| Matrix tension | $\delta_{mt,eq} = L_C\sqrt{< \varepsilon_{22} >^2 + \varepsilon_{12}^2 + \varepsilon_{23}^2}$ | $\sigma_{mt,eq} = \frac{L_C(< \sigma_{22} >< \varepsilon_{22} > + \sigma_{12}\varepsilon_{12} + \sigma_{23}\varepsilon_{23}}{\delta_{mt,eq}}$ |
| Matrix compression | $\delta_{mc,eq} = L_C\sqrt{< -\varepsilon_{22} >^2 + \varepsilon_{12}^2}$ | $\sigma_{mc,eq} = \frac{L_C(< -\sigma_{22} >< -\varepsilon_{22} > + \sigma_{12}\varepsilon_{12})}{\delta_{mc,eq}}$ |

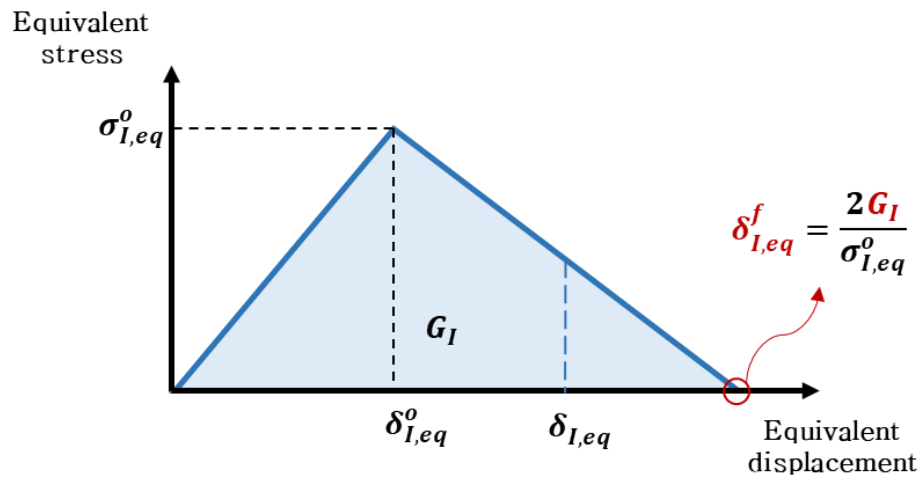


**Figure 3.1 Equivalent displacement and stress relation with the fracture energy**

## 3.3. Damage material constitutive law

FRPMC is considered as an orthotropic material that has the constitutive law as follows

$$\sigma_{ij} = C_{ijkl}\varepsilon_{kl} \tag{23}$$

The damage variables play an important role in material softening behavior after failure is initiated. Effect of damage variables in Continuum Damage Mechanics (CDM) model were firstly studied by Kachanov [1]. Here, the concept of the stiffness degradation was based on Matzenmiller et al. [24] and Murakami et al. [31]. This model illustrates the relation between nominal stress σ and effective

stress $\hat{\sigma}$ with the damage operator M.

$$\hat{\boldsymbol{\sigma}} = \mathbf{M}\boldsymbol{\sigma} \tag{24}$$

$$\mathbf{M} = \begin{bmatrix} \frac{1}{d_f} & & & & & & \\ & \frac{1}{d_m} & & & & & \\ & & 1 & & & & \\ & & & \frac{1}{d_f d_m} & & & \\ & & & & \frac{1}{d_f} & & \\ & & & & & \frac{1}{d_m} & \end{bmatrix} \tag{25}$$

The term damage variables $d_f$ and $d_m$ used in Eq. (25) have the following relation

$$\boldsymbol{d_f} = (\mathbf{1} - \boldsymbol{d_{ft}})(\mathbf{1} - \boldsymbol{d_{fc}}) \tag{26}$$

$$\mathbf{d_m} = (\mathbf{1} - \boldsymbol{d_{mt}})(\mathbf{1} - \boldsymbol{d_{mc}}) \tag{27}$$

The damage variable corresponding to shear is assumed depending on other variables.

$$d_s = d_f d_m \tag{28}$$

The present CDM model is the same as that of previous researches [32-34]. The damaged compliance matrix S(d) can be

expressed in Table 3.2. Engineering constants such as $\mathrm{E}_1, E_2, E_3, G_{12}, G_{13}, G_{23}, \nu_{12}, \nu_{13}, \nu_{23}$ denote undamaged constants.

## 3.4. Viscous regularization technique

Prediction of softening behavior due to tangent stiffness degradation often has a convergence issue in the implicit analysis. To avoid the convergence problem, a viscous regularization technique was adopted. Tangent stiffness matrix of such material behavior is positive definite using this approach.

**Table 3.2. Damaged compliance and constitutive tensor**

| | |
|---|---|
| $\mathbf{C(d)}$ | $\frac{1}{\Delta}\begin{bmatrix} d_f E_{11}(1-d_m\nu_{23}\nu_{32}) & d_f d_m E_{11}(\nu_{21}+\nu_{23}\nu_{31}) & d_f E_{11}(\nu_{31}+\nu_{21}\nu_{32}) & & & \\ & d_m E_{22}(1-d_f\nu_{13}\nu_{31}) & d_m E_{22}(\nu_{32}+d_f\nu_{12}\nu_{31}) & & & \\ & & E_{33}(1-d_m d_f\nu_{12}\nu_{21}) & & & \\ & & & \Delta d_f d_m G_{12} & & \\ & sym & & & \Delta d_f G_{13} & \\ & & & & & \Delta d_m G_{23} \end{bmatrix}$ <br> $\Delta = 1 - \mathrm{d_f} d_m \nu_{12}\nu_{21} - d_m\nu_{23}\nu_{32} - d_f\nu_{13}\nu_{31} - 2d_f d_m \nu_{21}\nu_{32}\nu_{13}$ |
| $\mathbf{S(d)}$ | $\begin{bmatrix} \frac{1}{d_f E_1} & -\frac{\nu_{21}}{E_{22}} & -\frac{\nu_{31}}{E_{33}} & & & \\ & \frac{1}{d_m E_{22}} & -\frac{\nu_{32}}{E_{33}} & & & \\ & & \frac{1}{E_{33}} & & & \\ & & & \frac{1}{d_f d_m G_{12}} & & \\ & sym & & & \frac{1}{d_f G_{13}} & \\ & & & & & \frac{1}{d_m G_{23}} \end{bmatrix}$ |

This regularization scheme is the Duvaut and Lions [35] model. A damage variable with viscous regularization is defined as follows

$$\dot{d}_I^v = \frac{1}{\eta_I}(d_I - d_I^v) \tag{29}$$

In this equation, the super script $v$ denotes viscous regularized variable, $I$ is each damage mode and $\eta$ denotes a viscosity coefficient with respect to relaxation time.

The value of the viscosity coefficient is usually small for time increment. This relation between the viscosity coefficient and time increment helps to alleviate the convergence problem.

## 3.5. Numerical implementation

User-defined material model (UMAT) was implemented to use finite element solver in commercial software ABAQUS/standard. The user-subroutine UMAT has been written in FORTRAN.

Twenty seven state variables are defined in the UMAT: one material state variable, four value for failure criterion calculation, five damage variable, five viscous damage variable and four equivalent

displacements of current step, damage onset and ultimate damaged state respectively. Twenty two state variables were used for calculations. Five state variables of viscous damage variable is listed in Table 3.3.

Strain, state variable array and characteristic length of the element were passed into UMAT. The first part of UMAT subroutine is the failure criteria.

It is followed by calculations of the equivalent displacements. If previous failure criterion value is 0 and the current value equal to 1, this state implies damage initiation. When the failure criterion was firstly satisfied, the equivalent displacement and stress were calculated once and stored as the state variables for the sake of computational efficiency.

Finally, UMAT requires updates of the stress and tangent stiffness for the modified stress and construct the stiffness matrix at every material integral point. Accurate tangent stiffness plays an important role in the implicit analysis. Analytical derivation of the tangent stiffness can be expressed as follows

$$\frac{\partial \boldsymbol{\sigma}}{\partial \boldsymbol{\varepsilon}} = \boldsymbol{C}(\boldsymbol{d_I}) + \boldsymbol{\varepsilon} : \sum_{\boldsymbol{I}} \frac{\partial \boldsymbol{C}(\boldsymbol{d_I^v})}{\partial \boldsymbol{d_I^v}} \frac{\partial \boldsymbol{d_I^v}}{\partial \boldsymbol{d_I}} \frac{\partial \boldsymbol{d_I}}{\partial \boldsymbol{\varepsilon}} \quad \textbf{(30)}$$

The tangent stiffness consists of damaged constitutive tensor and viscous damage variables. The partial derivative term in the Eq. (30) can be calculated easily. However, Eq. (29) only shows the regularization regime. The equation was modified to a computational form in order to implement Eq. (30). The computational form of the viscous regularization have a relation as follows

$$\boldsymbol{d_I^v}|_{\boldsymbol{t_0+\Delta t}} = \frac{\boldsymbol{\Delta t}}{\boldsymbol{\eta_I + \Delta t}} \boldsymbol{d_I}|_{\boldsymbol{t_0+\Delta t}} + \frac{\boldsymbol{\eta_I}}{\boldsymbol{\eta_I + \Delta t}} \boldsymbol{d_I^v}|_{\boldsymbol{t_0}} \quad \textbf{(31)}$$

Where, $\frac{\boldsymbol{\Delta t}}{\boldsymbol{\eta}} > \mathbf{1}$

Consequently, the partial derivative of the viscous damage variable with respect to damage variable can be calculated by Eq. (32).

$$\frac{\partial \boldsymbol{d_I^v}}{\partial \boldsymbol{d_I}} = \frac{\boldsymbol{\Delta t}}{\boldsymbol{\eta_I + \Delta t}} \quad \textbf{(32)}$$

A flow chart of UMAT is depicted in Figure 3.2.

To verify the UMAT, a simple cantilever beam FE model was

generated. Progressive damage analysis was carried out under unidirectional displacement loading. Boundary conditions and required material properties are listed in Figure 3.3. The stress–strain curve illustrates reasonable results under uniaxial loading. Figure 3.4 illustrates how UMAT works in the FE model.

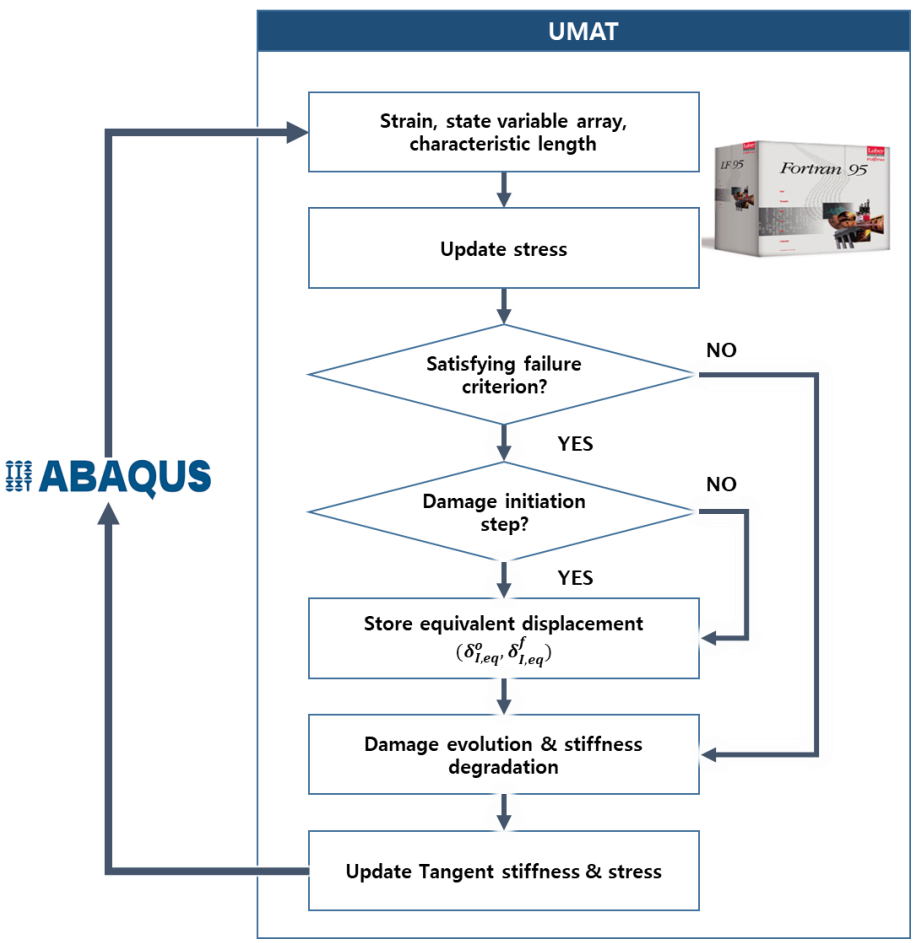


**Figure 3.2 flow chart of user-define material (UMAT)**

## A. FE Model

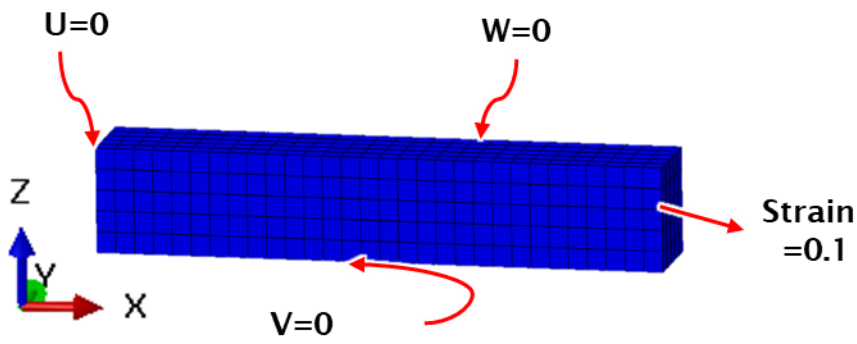


## B. Material properties

| $E_{11}$ (MPa) | $E_{22=33}$ (MPa) | $v_{12=13}$ | $v_{23}$ | $G_{12=13}$ (MPa) | $G_{23}$ (MPa) |
|---|---|---|---|---|---|
| 200451 | 11438 | 0.29 | 0.512 | 8963 | 3783 |

| $F_{1t}$ (MPa) | $F_{1c}$ (MPa) | $F_{2t}$ (MPa) | $F_{2c}$ (MPa) | $F_{ls}$ (MPa) | $F_{ts}$ (MPa) |
|---|---|---|---|---|---|
| 4270.5 | 3843 | 112.7 | 218.7 | 82 | 81 |

| $G_{ft}$ $(J/mm^2)$ | $G_{fc}$ $(J/mm^2)$ | $G_{mt}$ $(J/mm^2)$ | $G_{mc}$ $(J/mm^2)$ |
|---|---|---|---|
| 100 | 100 | 5 | 5 |

**Figure 3.3 Verification finite element model and material properties**

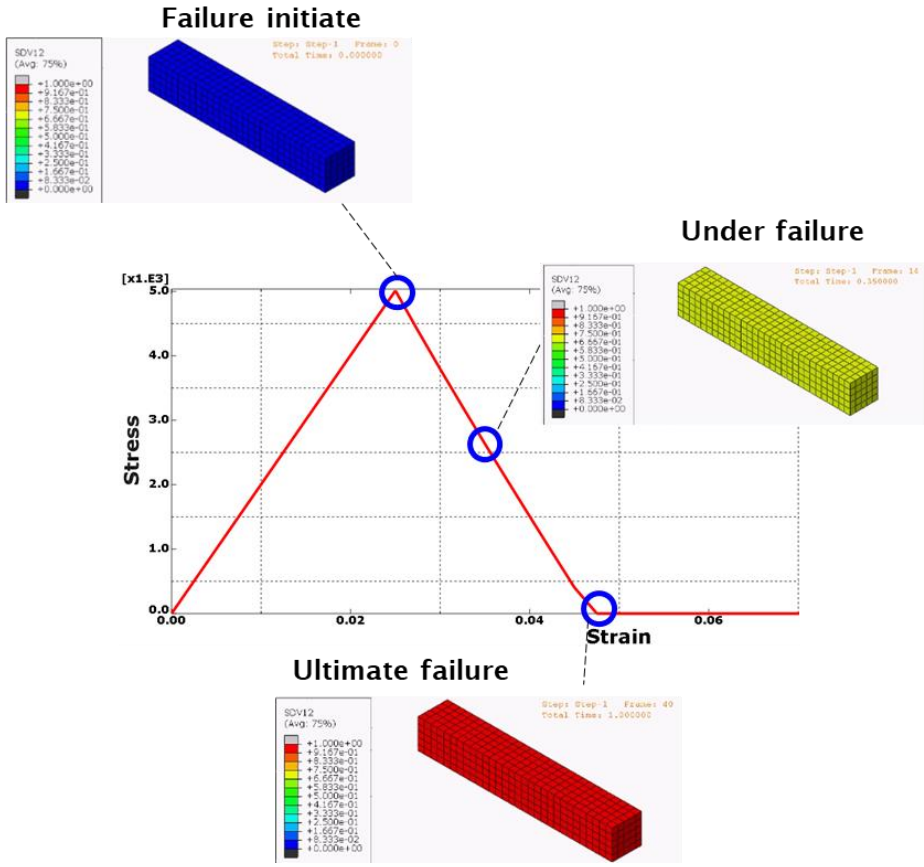


**Figure 3.4 Stress-strain curve with the viscous damage variable**

**Table 3.3 State variables related to damage variables**

| State variable | 11 | 12 | 13 | 14 | 15 |
|---|---|---|---|---|---|
| Damage variable | $d_s^v$ | $\mathrm{d}_{\mathrm{ft}}^{\mathrm{v}}$ | $\mathrm{d}_{\mathrm{fc}}^{\mathrm{v}}$ | $\mathrm{d}_{\mathrm{mt}}^{\mathrm{v}}$ | $\mathrm{d}_{\mathrm{mc}}^{\mathrm{v}}$ |

## 3.6. Verification of UMAT

ABAQUS user subroutine (UMAT) was implemented in the previous section. A thin single layer model was generated for the sake of verification in Figure 3.5. Glass fiber-reinforced polymer(GFRP) was used in the FE model and material properties for UMAT are listed from Table 3.4 to Table 3.6 [13]. Two-dimensional square S4 element was adopted for the built-in material model. Three-dimensional hexagonal element C3D8 was used in UMAT. The orientation of fiber was aligned in x axis. The quarter model using symmetric condition was generated for progressive damage analysis. The displacement boundary condition was applied

The fiber tension and compression damage variable were not shown in this model. The state variable 14 and 15 that represent matrix tension and compression damage variable respectively at time t=0.875 and t=1 were shown in Figure 2.6 and Figure 2.7. The results of progressive damage analysis with UMAT have similar results of built-in material. The damage variable has upper limit value as 1. The contour of each variable has more than 1 due to extrapolation because UMAT was calculated at the integration point.

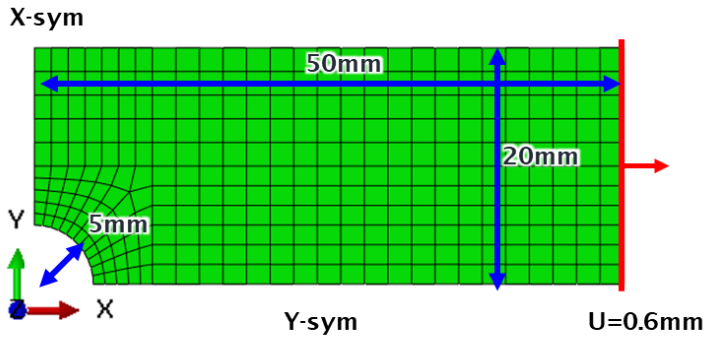


**Figure 3.5. FE model of thin single layer for verification of UMAT**

**Table 3.4. Orthotropic properties of fiber reinforced epoxy. [13]**

| $E_{11}$ (MPa) | $E_{22=33}$ (MPa) | $\nu_{12=13}$ | $\nu_{23}$ | $G_{12=13}$ (MPa) | $G_{23}$ (MPa) |
|---|---|---|---|---|---|
| 55000 | 9500 | 0.33 | 0.2 | 5500 | 3000 |

**Table 3.5. Strength of fiber reinforced epoxy. [13]**

| $F_{1t}$ (MPa) | $F_{1c}$ (MPa) | $F_{2t}$ (MPa) | $F_{2c}$ (MPa) | $F_{ls}$ (MPa) | $F_{ts}$ (MPa) |
|---|---|---|---|---|---|
| 2500 | 2000 | 50 | 150 | 50 | 50 |

**Table 3.6. Fracture energies for fiber reinforced epoxy [13]**

| $G_{ft}$ $(J/mm^2)$ | $G_{fc}$ $(J/mm^2)$ | $G_{mt}$ $(J/mm^2)$ | $G_{mc}$ $(J/mm^2)$ |
|---|---|---|---|
| 12.5 | 12.5 | 1 | 1 |

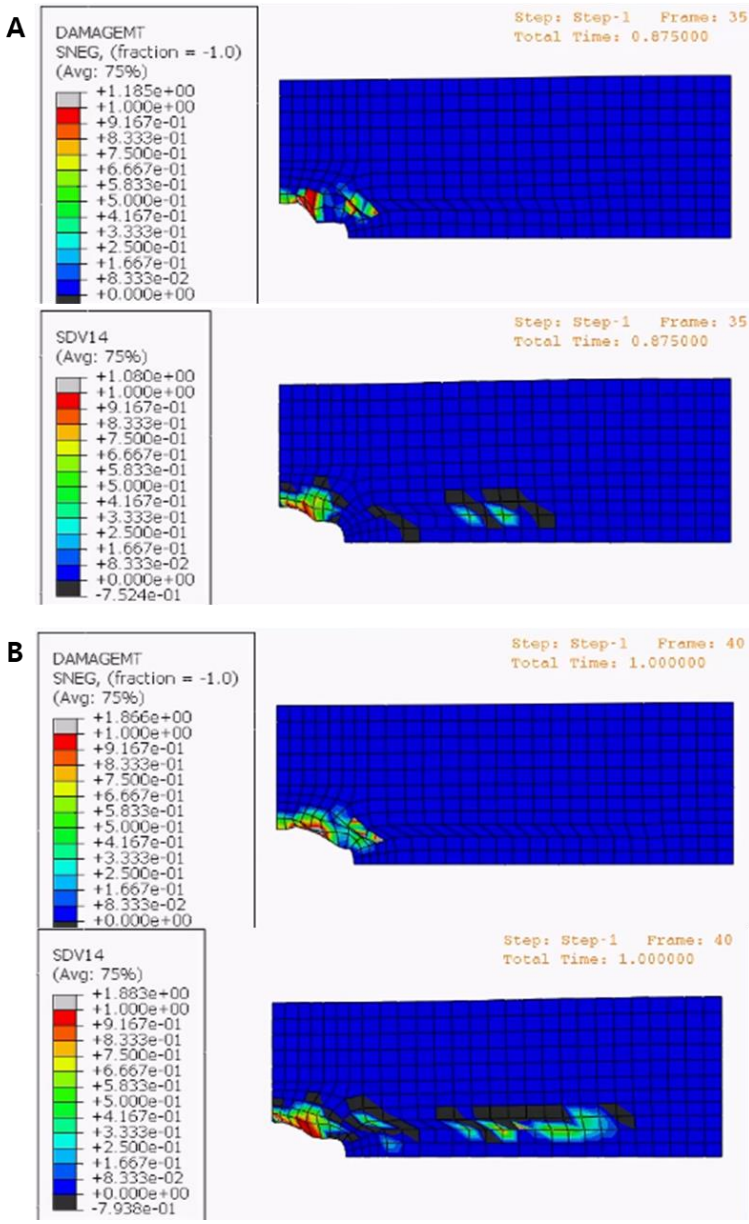


**Figure 3.6. Matrix tension damage contour at A) time t =0.875 and B) t=1**

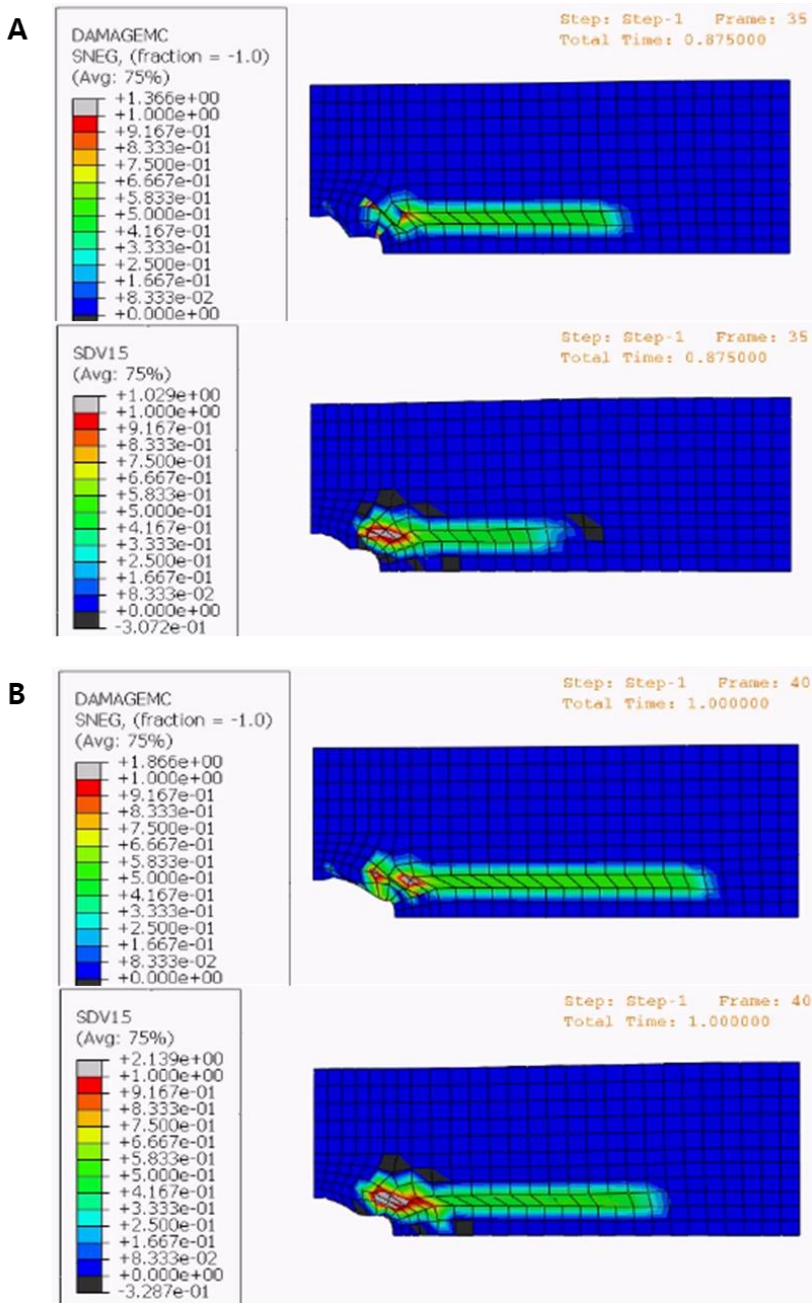


**Figure 3.7 Matrix compression damage contour at A) time t =0.875 and B) t=1**

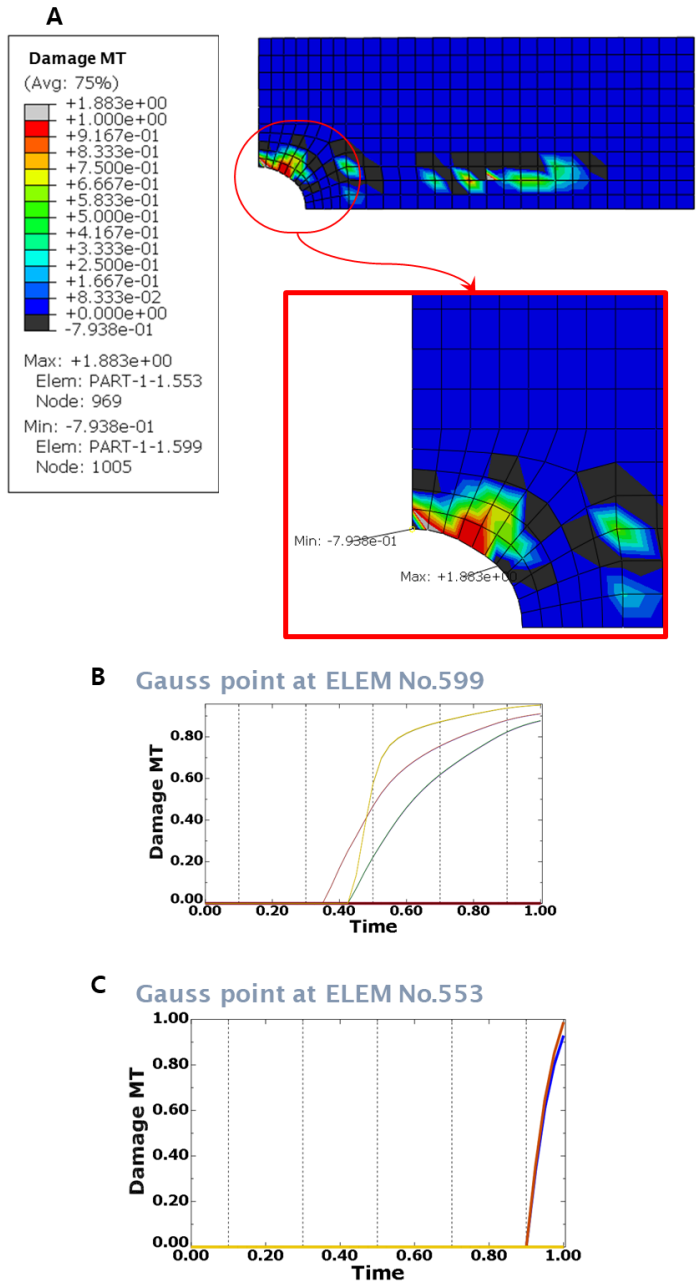


**Figure 3.8. Damage variable of matrix tension at A) FE model, B) element which have minimum value and C) maximum value**

## 3.7. Stochastic damage material model

KL expansion was combined with progressive damage model for the sake of considering spatial material defects. This thesis utilized ABAQUS for these computational stochastic progressive damage model.

The governing equation for mechanical problems was given in Eq.

$$\sigma_{ij,x_j} + b_i = 0 \tag{33}$$

where $b_i$ represents body force.

Using the hook's law and KL expansion, the governing equation can be expressed as following Eq. (34), (35)

$$C(d^v, \omega) \tag{34}$$

$$\left(C(d^v, \omega)\epsilon_{ij}\right)_{,xj} + b_i = 0 \tag{35}$$

Eq. (35) represents governing equation with spatial material constitutive mode. Figure 3.9 illustrate Eq.(35) under the domain.

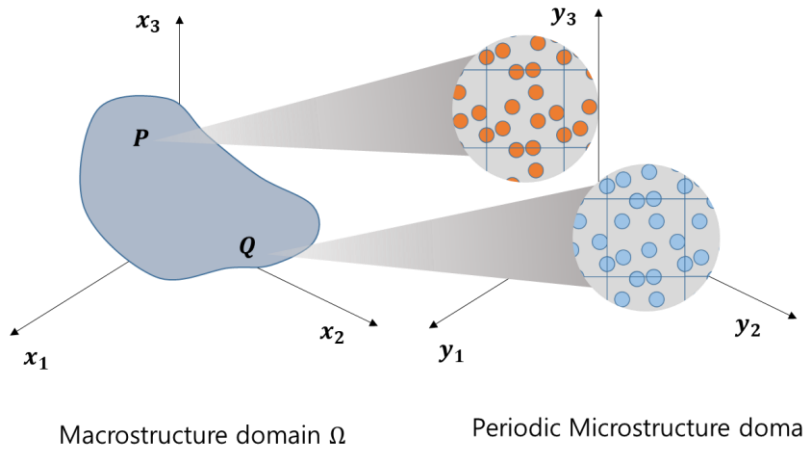


**Figure 3.9 Macroscale and microscale domain with spatial material different**

# 4. Numerical examples

## 4.1. A progressive damage analysis

The FE model of open hole model was generated. This model has 50mm length, 20mm height and 1 mm thickness as Figure 4.1

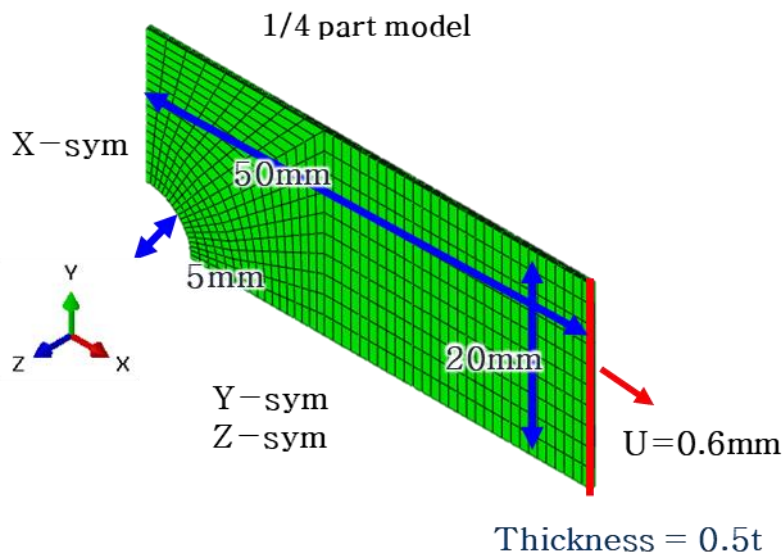


**Figure 4.1 Quarter FE model**

Quarter FE model was generated using symmetric boundary condition. Symmetric layup [0/90/0/90] was adopted through-thickness. Each ply has thickness 0.125mm. The detailed layup was

shown as following Figure 4.2

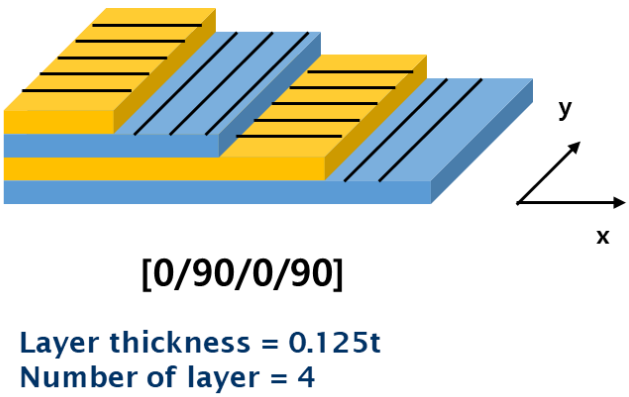


**Figure 4.2 Through-thickness layup of laminate**

Material properties which have same value from Table 3.4 to Table 3.6 were used.

Progressive damage analysis without material spatial distribution was conducted as following Figure 4.3.

Fiber related damage variables were not show under this loading condition. Each ply has different damage contour. In the 90° layer, matrix tension damage is more dominant due to fiber aligned in y axis.

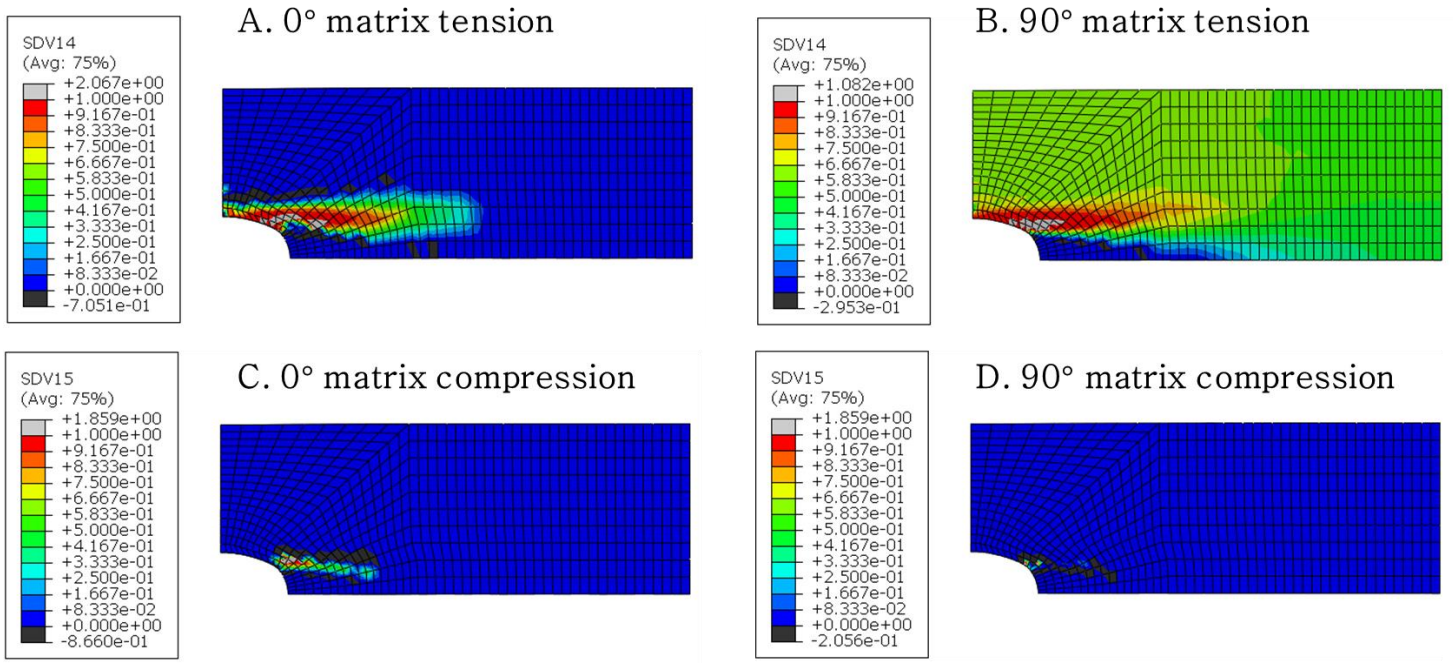


**Figure 4.3 Viscous damage variables of each layer**

## 4.2. Effects of spatial strength

The rotational tensor with angle $\theta = 90°, \phi = 0°$ and $\theta = 90°, \phi = 90°$ was used for fiber orientation of $0°$ and $90°$ respectively. Because Hashin failure criterion includes material strength and material strength is generally defines by experiments. Strength was considered as random field variable. Non-uniform strength distribution affects when the failure onset. Orientation angle and correlation length were listed in Table 4.1.

**Table 4.1 Orientation angle and correlation length for kl expansion**

| | $\boldsymbol{\theta}$ | $\boldsymbol{\phi}$ | $\boldsymbol{L_{cx}}$ | $\boldsymbol{L_{cy} = L_{cz}}$ |
|---|---|---|---|---|
| 0° layer | 90 | 0 | 50 | 5 |
| 90° layer | 90 | 90 | 50 | 5 |

Generally, correlation length was hard to define. Correlation length was assumed as same length of RVE. Ten times of model's characteristic length was assumed for the fiber direction. Same length was used for transverse direction.

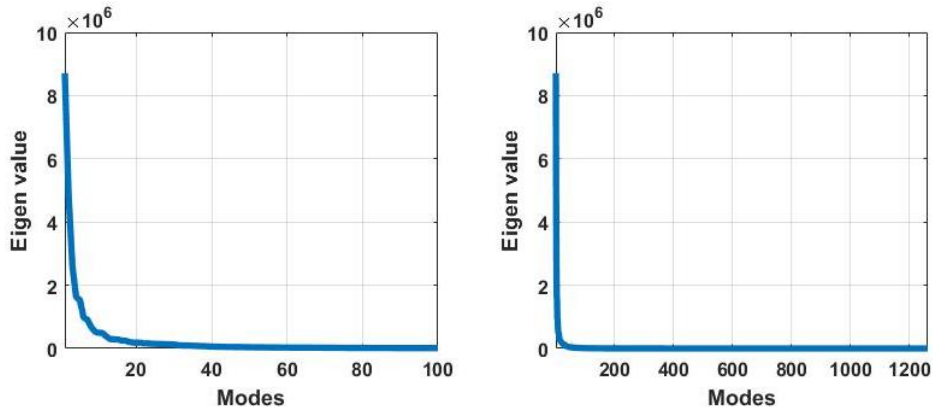


**Figure 4.4 descending eigenvalue with truncation**

In above Figure 4.4, truncated eigenmodes were adopted for computational efficiency instead of total eigenmodes. 97% value of total summation of the eigenvalue was used in this simulation.

Six different strength were modeled with following Table 4.2.

**Table 4.2 Statistical parameter of six strength**

| | $F_{1t}$ (MPa) | $F_{1c}$ (MPa) | $F_{2t}$ (MPa) | $F_{2c}$ (MPa) | $F_{ls}$ (MPa) | $F_{ts}$ (MPa) |
|---|---|---|---|---|---|---|
| mean | 2500 | 2000 | 50 | 150 | 50 | 50 |
| cov | 0.1 | 0.1 | 0.1 | 0.1 | 0.1 | 0.1 |

Due to lack of experimental data, coefficient of variance was assumed as 0.1.

Strength related to each damage mode can be expressed as

follow

$$F_N(\vec{P}) = \ < T(\vec{P}) > \ + \ \sum_{i=1}^{m=200} \sqrt{\lambda_i}\, \phi_i(\vec{P})[\xi_i] \qquad \textbf{(36)}$$

where N is $\mathrm{F}_{1\mathrm{t}}, F_{1c}, F_{2t}, F_{2c}, F_{ls}$ and $F_{ts}$

Ten different samples were generated with KL expansion. Spatial distribution of fiber tension strength was shown in Figure 4.5. The second layer of each orientation has a similar spatial material contour to the first layer.

Progressive damage analysis of 1 reference model and 10 randomly sampled model were carried out. From Figure 4.6 to Figure 4.9, the results of stochastic FE analysis were shown

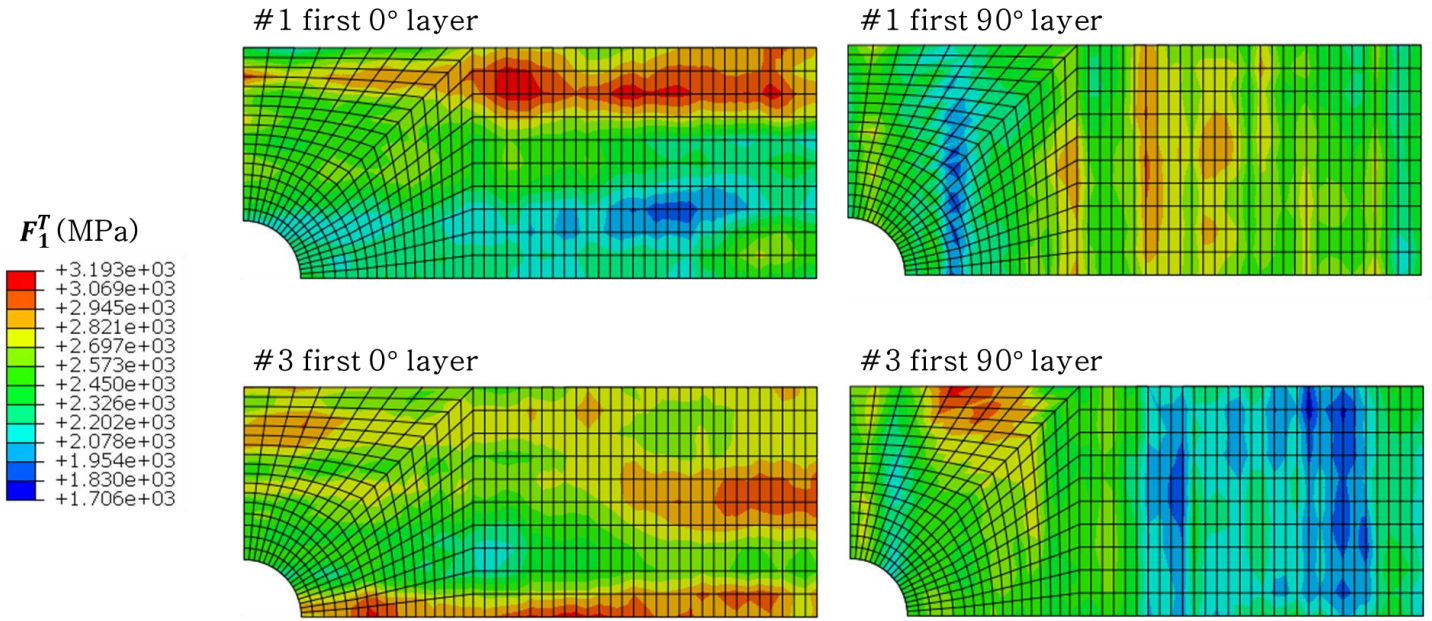


**Figure 4.5 Material spatial distribution at each layer of two sample**

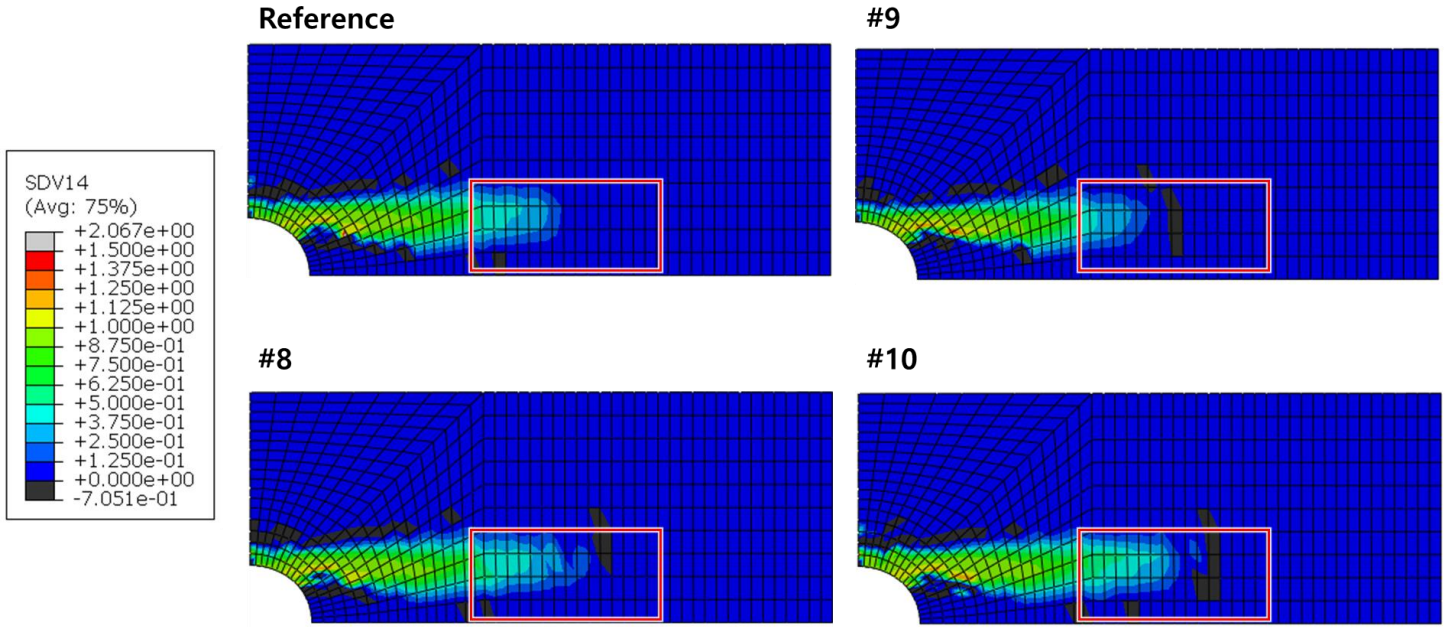


**Figure 4.6 Viscous damage variable of matrix tension at 0 degree layer**

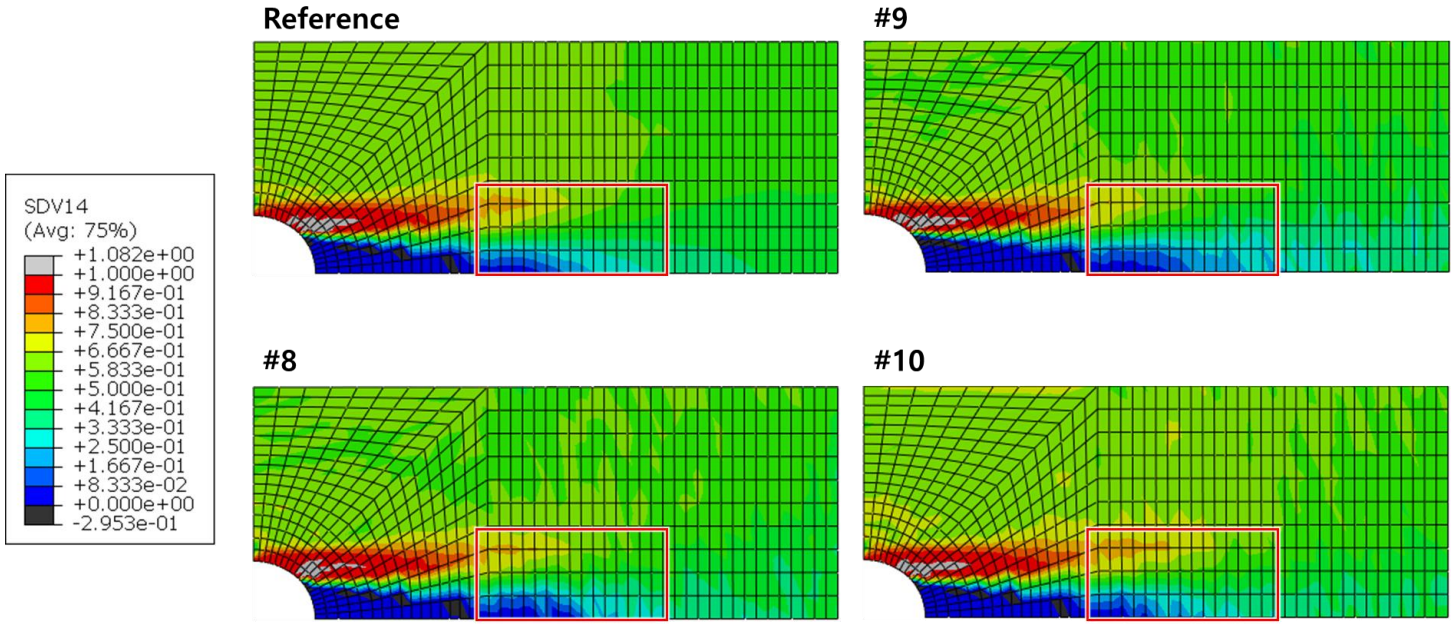


**Figure 4.7 Viscous damage variable of matrix tension at 90 degree layer**

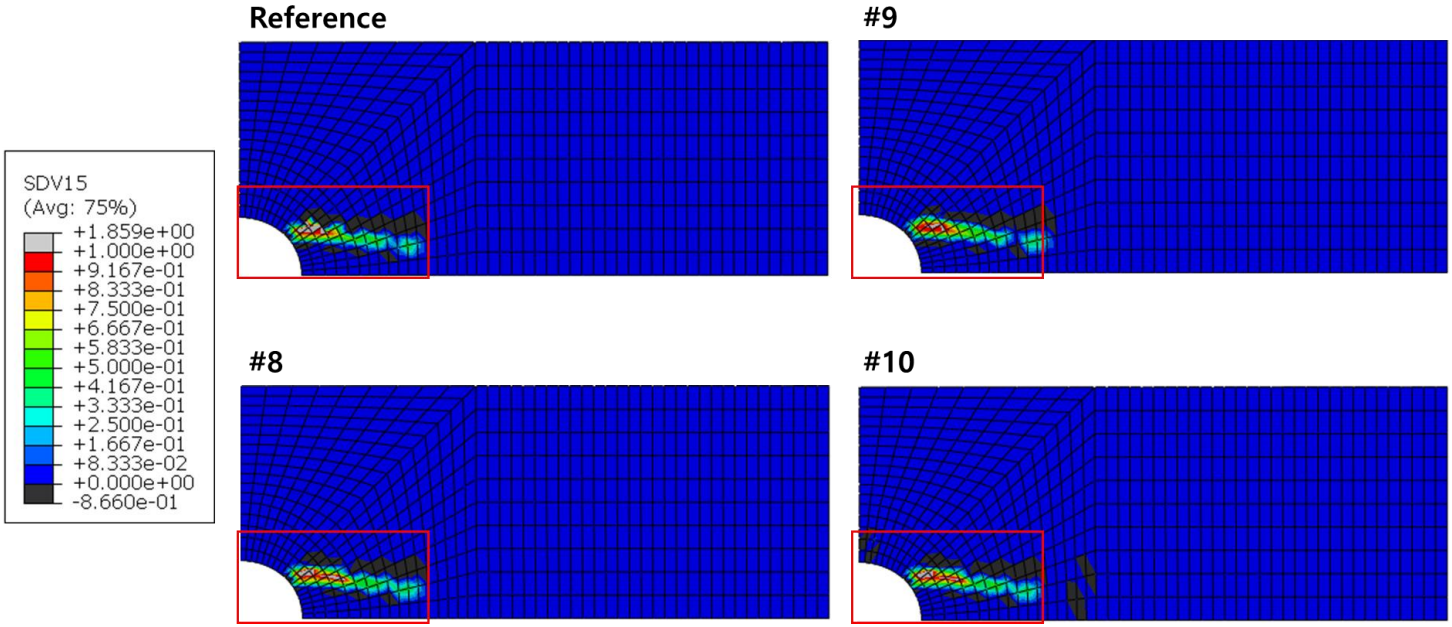


**Figure 4.8 Viscous damage variable of matrix compression at 0 degree layer**

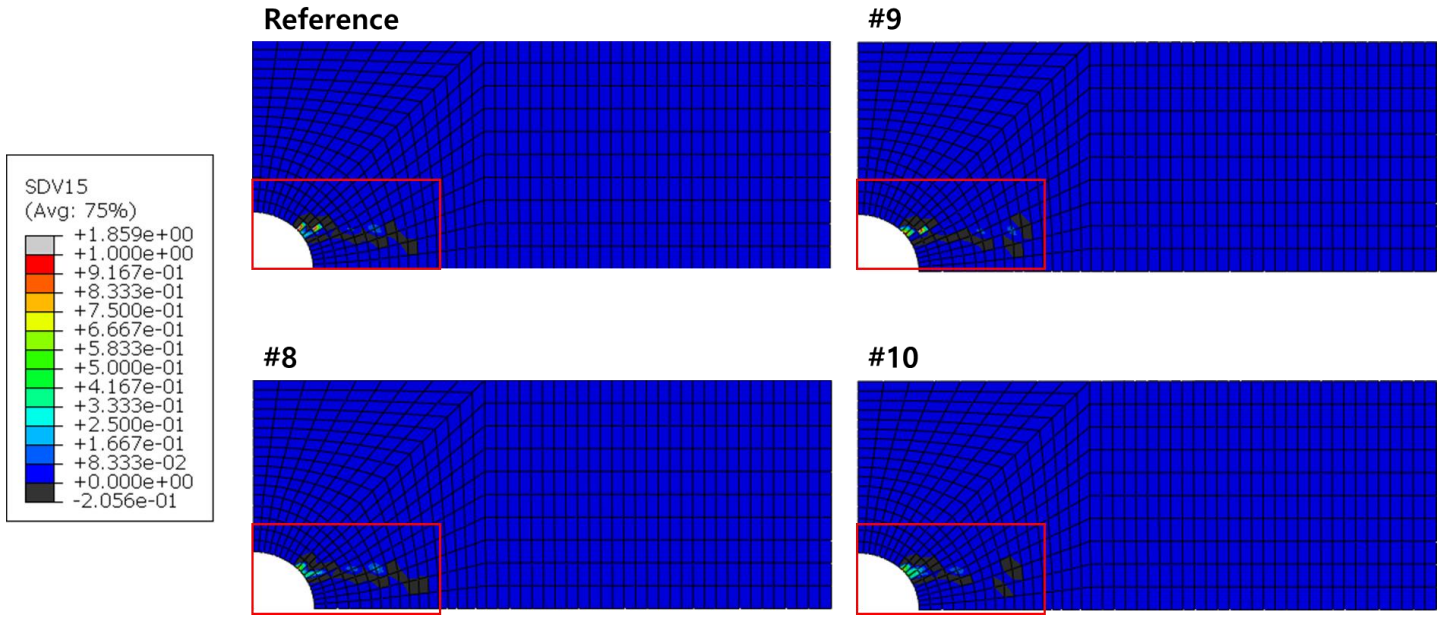


**Figure 4.9 Viscous damage variable of matrix compression at 90 degree layer**

Using the kl expansion method, the damaged pattern with different spatial location were obtained according to the above figures.

Elemental averaged stress−strain curve were calculated in the region depicted in Figure 4.10

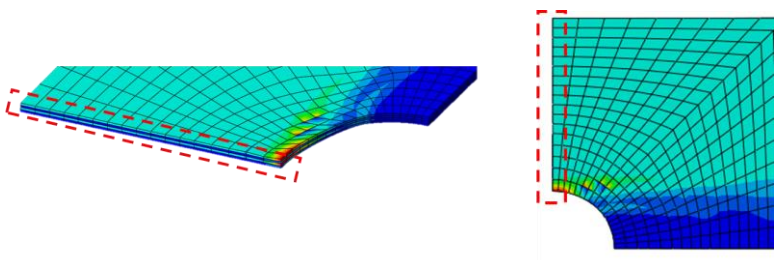

**Figure 4.10 Section of FE model for stress-strain curve**

Averaged stress and strain were calculated as follow

$$\sigma' = \frac{\sum \sigma V}{\sum V}, \qquad \epsilon' = \frac{\sum \epsilon V}{\sum V} \tag{37}$$

where ′ indicates averaged value; and V indicates elemental volume.

Both stress−strain curves were given in Figure 4.11 and Figure 4.12.

The initiation of damage varied significantly in $\sigma_{22} - \epsilon_{11}$.

Each sample have similar $\sigma_{11} - \epsilon_{11}$ curve. Fiber damage did not occur under this loading.

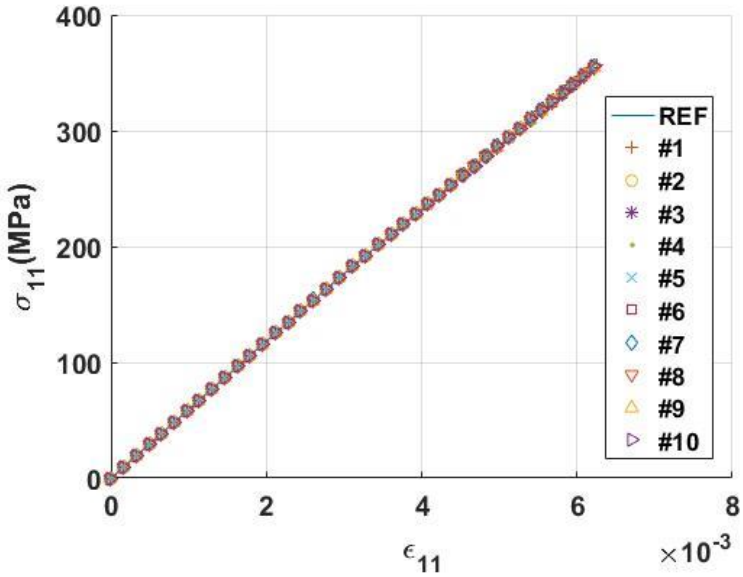


**Figure 4.11 $\sigma_{11} - \epsilon_{11}$ curve of stochastic strength**

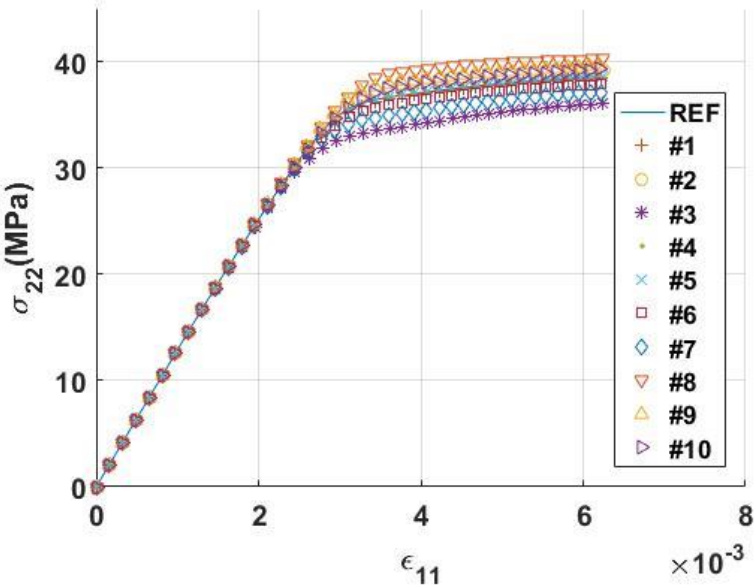


**Figure 4.12 $\sigma_{22} - \epsilon_{11}$ curve of stochastic strength**

## 4.3. Effects of spatial fracture energy

A spatial fracture energy can cause spatially different ultimate damage state. The concept of the stochastic fracture energy is given in Figure 4.13.

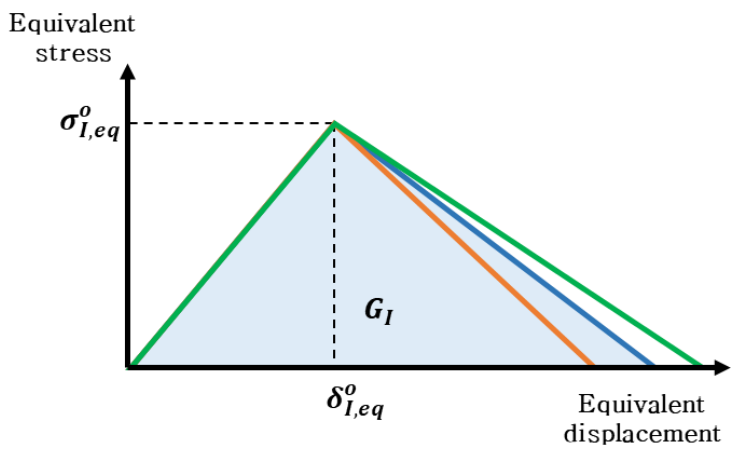


**Figure 4.13 a stochastic fracture energy**

To investigate effect of fracture energy, four different fracture energy were modeled as random field variable as listed in

**Table 4.3 a statistical parameter of fracture energy**

| | $G_{ft}$ $(J/mm^2)$ | $G_{fc}$ $(J/mm^2)$ | $G_{mt}$ $(J/mm^2)$ | $G_{mc}$ $(J/mm^2)$ |
|---|---|---|---|---|
| mean | 12.5 | 12.5 | 1 | 1 |
| cov | 0.1 | 0.1 | 0.1 | 0.1 |

The strength was assumed to be deterministic. Each fracture energy was assumed to follow the normal distribution. Orientation angle and correlation length have same value as listed in Table 4.1.

To consider the effects of spatial fracture energy volume averaged stress and stress was adopted. The results of reference model and each sample was shown in Figure 4.14.

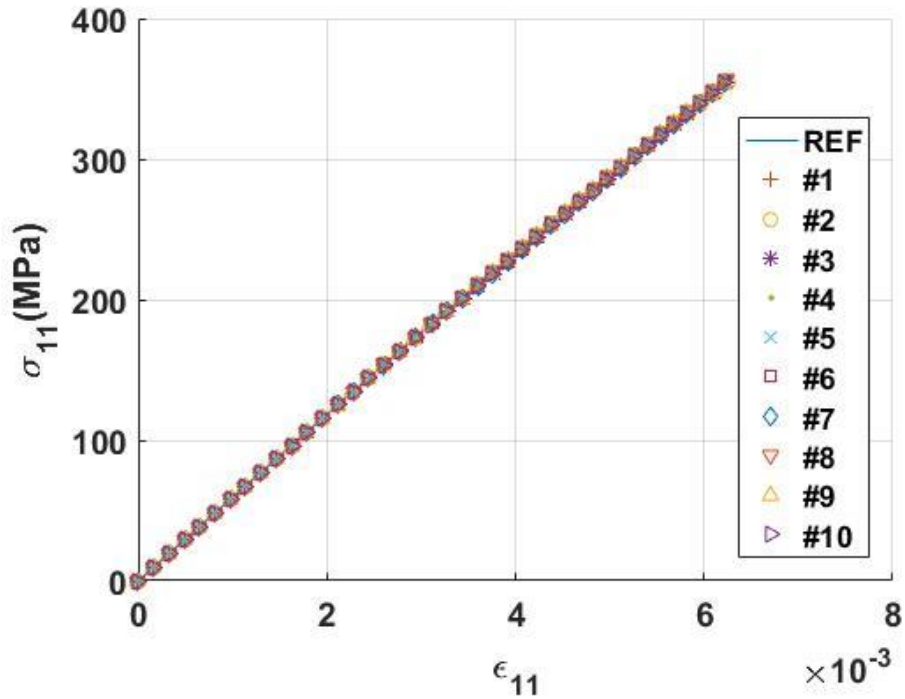


**Figure 4.14 $\sigma_{11} - \epsilon_{11}$ curve of stochastic fracture energy**

Figure 4.14 shows stress-strain relation that have similar results compared to spatial strength.

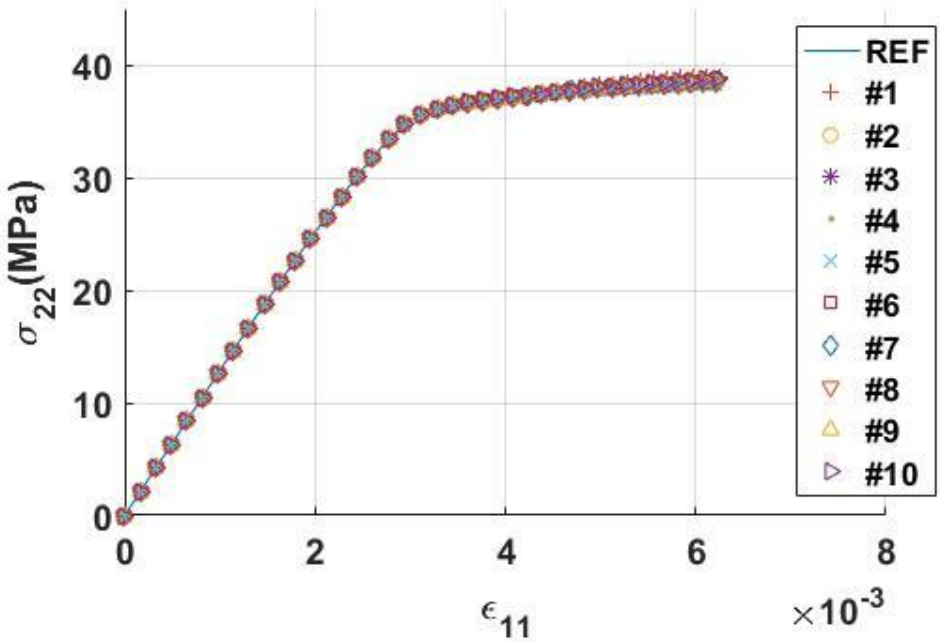


**Figure 4.15 $\sigma_{22} - \epsilon_{11}$ curve of stochastic fracture energy**

Figure 4.15 illustrates that damage onset was not varied and the slope of stress–strain curve after damage slightly changed.

## 4.4. Effects of spatial fracture energy with cohesive elements

Delamination is important damage mode in lamina structure. Cohesive layer was generated between two layers. COH3D8 element was used for cohesive layer. The detailed layer is given in Figure 4.16

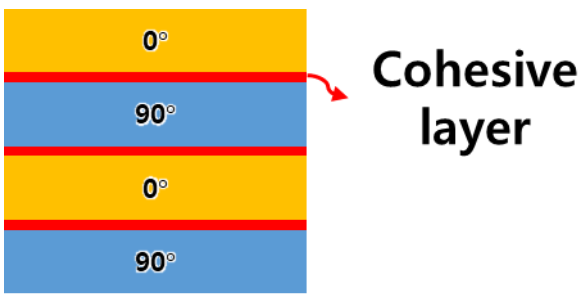


**Figure 4.16 Laminate layup with cohesive layer**

The thickness of a cohesive layer is 0.001 which is 1% of each layer. COH3D8 elements was used for adhesive region. The material properties of cohesive elements from lapczyk [13] was shown in

**Table 4.4 Material properties of the cohesive element [13]**

| $E_{11}$(MPa) | ν | $t_n^f$(MPa) | $t_s^f$(MPa) | $G_n$ (N/mm) | $G_s$(N/mm) |
|---|---|---|---|---|---|
| 2000 | 0.33 | 50 | 50 | 4.0 | 4.0 |

Where $t_n^f$ and $t_s^f$ are the peak strength; and $G_n$ and $G_s$ are fracture

energies of cohesive element.

The stochastic progressive damage model of reference model and ten different samples was carried out. The material distribution is same to the distribution of previous section 4.3. To investigate the effects of the cohesive elements, volume averaged stress–strain curve was given in Figure 4.17 and Figure 4.18

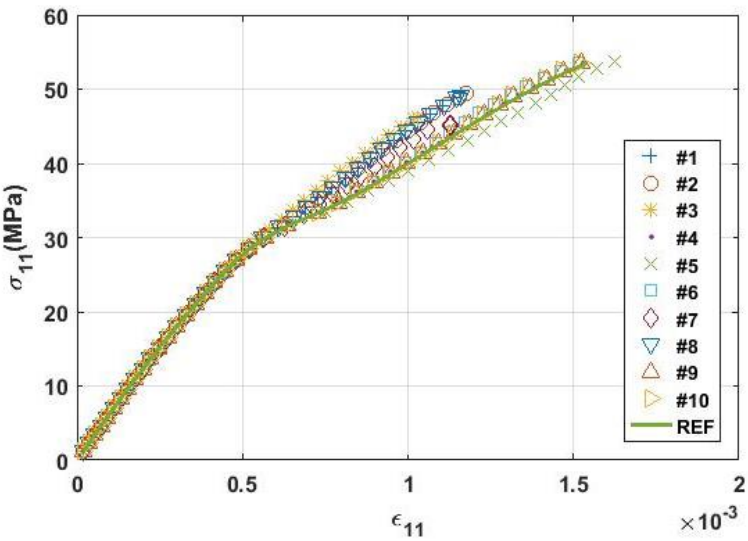


**Figure 4.17 $\sigma_{11} - \epsilon_{11}$ curve of stochastic fracture energy with cohesive element**

Above figure illustrates the effects of cohesive elements. The slope of the figure was changed due to the cohesive elements. After the damage onset of adhesive, the slope was changed because of the

spatial fracture energy.

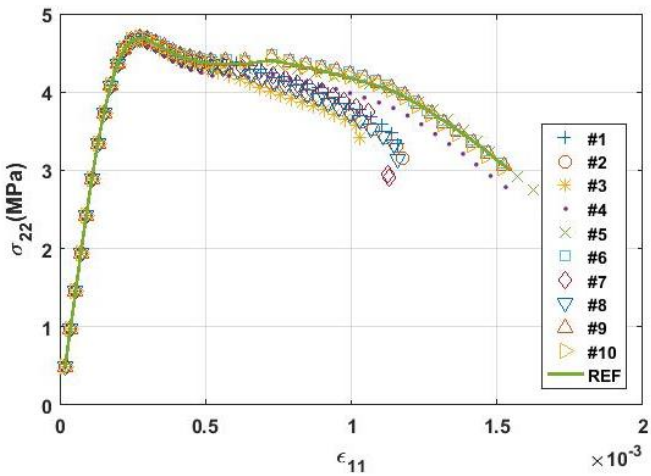


**Figure 4.18 $\sigma_{22} - \epsilon_{11}$ curve of stochastic fracture energy with cohesive element**

In this figure, two slope changes can be observed. The one is the change due to the cohesive element and the other is the change due to progressive damage of layer. Also, the spatial fracture energy do not affect the damage onset with cohesive layers.

# 5. Conclusion and future works

## 5.1. Conclusion

In this thesis, a stochastic progressive damage analysis model was developed to considering effects of spatial randomness of material. A progressive damage analysis model was based on continuum damage mechanics. This model considered four different damage modes: fiber tension, fiber compression, matrix tension, and matrix compression. Shear damage was depended on these four modes. The characteristic length was used to alleviate mesh dependency. Viscous regularization model was adopted to avoid convergence problem. Commercial software ABAQUS have the only two-dimensional material model. In order to apply three-dimensional progressive damage analysis, user-subroutine for stochastic progressive damage analysis was implemented. UMAT was verified compared to a two-dimensional built-in material

Three-dimensional Karhunen-Loeve expansion was derived considering fiber orientation and different correlation length. Strength plays important role in failure criterion. Six different

strength were modeled as random field variable. Four different fracture energy were also modeled as the random field.

The stress–strain curve illustrates the same properties before damage onset. After the damage initiation, each model has a different yielding point in case of spatial strength. Slight change can be obtained when spatially distributed fracture energy was used. Different damage pattern of each FE model can be obtained. Thin cohesive layer was generated inter layer region.

Composites material generally have a high standard deviation of the experimental results. This stochastic progressive damage analysis could improve the reliability of composite manufacturing. However, this model considered only intra lamina damage not inter lamina damage model.

## 5.2. Future works

In this thesis, some properties such as coefficient of variance and correlation length were assumed. The proposed progressive damage model with material spatial randomness need experimental validation,

which is another topic for further research.

Zero-thickness cohesive elements generally used for delamination. Material properties related cohesive elements also can be modeled as random field variable.

Micro scale structure was not considered in this thesis, Micromechanics have many uncertainties such as volume fraction and undulation of fiber. Their bridging to macro properties should also be considered for further research.

# 6. Reference


[1] L. Kachanov, "On the time to failure under creep conditions, Izv," *AN SSSR, Otd. Tekhn. Nauk,* vol. 8, no. 26-31, p. 8, 1958.

[2] P. Ladeveze and J. Lemaitre, "Damage effective stress in quasi unilateral conditions," in *16th International congress of theoretical and applied mechanics, Lyngby, Denmark*, 1984.

[3] R. Talreja, "Stiffness Properties of Composite Laminates with Matrix Cracking and Interior Delamination," (in English), *Engineering Fracture Mechanics,* vol. 25, no. 5-6, pp. 751-762, 1986.

[4] R. Talreja, *Damage Mechanics of Composite Materials* (Composite materials series 9). Amsterdam: Elsevier, 1994.

[5] F. Lene, "Damage Constitutive Relations for Composite-Materials," (in English), *Engineering Fracture Mechanics,* vol. 25, no. 5-6, pp. 713-728, 1986.

[6] D. H. Allen, C. E. Harris, and S. E. Groves, "A Thermomechanical Constitutive Theory for Elastic Composites with Distributed Damage .2. Application to Matrix Cracking in Laminated Composites," (in English), *International Journal of Solids and Structures,* vol. 23, no. 9, pp. 1319-1338, 1987.

[7] D. H. Allen, C. E. Harris, and S. E. Groves, "A Thermomechanical Constitutive Theory for Elastic Composites with Distributed Damage .1. Theoretical Development," (in English), *International Journal of Solids and Structures,* vol. 23, no. 9, pp. 1301-1318, 1987.

[8] E. J. Barbero and L. De Vivo, "A constitutive model for elastic damage in fiber-reinforced PMC laminae," (in English), *International Journal of Damage Mechanics,* vol. 10, no. 1, pp. 73-93, Jan 2001.

[9] P. Lonetti, R. Zinno, F. Greco, and E. J. Barbero, "Interlaminar damage model for polymer matrix composites," (in English), *Journal of Composite Materials,* vol. 37, no. 16, pp. 1485-1504, 2003.

[10] G. Z. Voyiadjis and P. I. Kattan, "Damage of Fiber-Reinforced Composite-Materials with Micromechanical Characterization," (in English), *International Journal of Solids and Structures,* vol. 30, no. 20, pp. 2757-2778, 1993.

[11] G. Z. Voyiadjis and T. Park, "The kinematics of damage for finite-strain elasto-plastic solids," (in English), *International Journal of Engineering Science,* vol. 37, no. 7, pp. 803-830, May 1999.

[12] G. Z. Voyiadjis and B. Deliktas, "A coupled anisotropic damage model for the inelastic response of composite materials," (in English), *Computer Methods in Applied Mechanics and Engineering,* vol. 183, no. 3-4, pp. 159-199, 2000.
[13] I. Lapczyk and J. A. Hurtado, "Progressive damage modeling in fiber-reinforced materials," *Composites Part A: Applied Science and Manufacturing,* vol. 38, no. 11, pp. 2333-2341, 2007.
[14] H. K. Jeong and R. A. Shenoi, "Reliability analysis of mid-plane symmetric laminated plates using direct simulation method," *Composite Structures,* vol. 43, no. 1, pp. 1-13, 1998/09/01/ 1998.
[15] B. Gentilleau, S. Villalonga, F. Nony, and H. Galiano, "A probabilistic damage behavior law for composite material dedicated to composite pressure vessel," *International Journal of Hydrogen Energy,* vol. 40, no. 38, pp. 13160-13164, 2015/10/15/ 2015.
[16] P. M. Scop and A. S. Argon, "Statistical Theory of Strength of Laminated Composites," *Journal of Composite Materials,* Article vol. 1, no. 1, pp. 92-99, 1967.
[17] S. Patel and C. Guedes Soares, "Reliability assessment of glass epoxy composite plates due to low velocity impact," *Composite Structures,* vol. 200, pp. 659-668, 2018/09/15/ 2018.
[18] C. Guedes Soares, "Reliability of components in composite materials," *Reliability Engineering and System Safety,* Article vol. 55, no. 2, pp. 171-177, 1997.
[19] N.-Z. Chen and C. Guedes Soares, "Spectral stochastic finite element analysis for laminated composite plates," *Computer Methods in Applied Mechanics and Engineering,* vol. 197, no. 51, pp. 4830-4839, 2008/10/15/ 2008.
[20] H. Jeong and R. Shenoi, "Probabilistic strength analysis of rectangular FRP plates using Monte Carlo simulation," *Computers & Structures,* vol. 76, no. 1-3, pp. 219-235, 2000.
[21] M. Chiachio, J. Chiachio, and G. Rus, "Reliability in composites - A selective review and survey of current development," *Composites Part B: Engineering,* vol. 43, no. 3, pp. 902-913, 2012/04/01/ 2012.
[22] W.-F. Wu, H.-C. Cheng, and C.-K. Kang, "Random field formulation of composite laminates," *Composite Structures,* vol. 49, no. 1, pp. 87-93, 2000.
[23] S. Jeong, F. Zhu, H. Lim, Y. Kim, and G. J. Yun, "3D stochastic computational homogenization model for carbon fiber reinforced CNT/epoxy composites with spatially random properties," *Composite Structures,* vol. 207, pp. 858-870, 2019/01/01/ 2019.
[24] A. Matzenmiller, J. Lubliner, and R. Taylor, "A constitutive model for anisotropic damage in fiber-composites," *Mechanics of materials,* vol.

20, no. 2, pp. 125-152, 1995.
[25] Z. Hashin, "Failure criteria for unidirectional fiber composites," *Journal of applied mechanics,* vol. 47, no. 2, pp. 329-334, 1980.
[26] J. P. Hou, N. Petrinic, C. Ruiz, and S. Hallett, "Prediction of impact damage in composite plates," *Composites Science and Technology,* vol. 60, no. 2, pp. 273-281, 2000.
[27] W. Guo, P. Xue, and J. Yang, "Nonlinear progressive damage model for composite laminates used for low-velocity impact," *Applied Mathematics and Mechanics,* vol. 34, no. 9, pp. 1145-1154, 2013.
[28] C. Zhang, N. Li, W. Wang, W. K. Binienda, and H. Fang, "Progressive damage simulation of triaxially braided composite using a 3D meso-scale finite element model," *Composite Structures,* vol. 125, pp. 104-116, 2015.
[29] C. Davila, N. Jaunky, and S. Goswami, "Failure criteria for FRP laminates in plane stress," in *44th AIAA/ASME/ASCE/AHS/ASC Structures, Structural Dynamics, and Materials Conference*, 2003, p. 1991.
[30] P. Maimí, P. P. Camanho, J.-A. Mayugo, and C. G. Dávila, "A thermodynamically consistent damage model for advanced composites," 2006.
[31] S. Murakami and K. Kamiya, "Constitutive and damage evolution equations of elastic-brittle materials based on irreversible thermodynamics," *International Journal of Mechanical Sciences,* vol. 39, no. 4, pp. 473-486, 1997.
[32] A. L. Highsmith and K. L. Reifsnider, "Stiffness-reduction mechanisms in composite laminates," in *Damage in Composite Materials: Basic Mechanisms, Accumulation, Tolerance, and Characterization*: ASTM International, 1982.
[33] N. Laws, G. J. Dvorak, and M. Hejazi, "Stiffness changes in unidirectional composites caused by crack systems," Cranfield Institute of Technology1983.
[34] R. Talreja, "Transverse cracking and stiffness reduction in composite laminates," *Journal of composite materials,* vol. 19, no. 4, pp. 355-375, 1985.
[35] G. Duvant and J. L. Lions, *Inequalities in mechanics and physics*. Springer Science & Business Media, 2012.

국문초록

# 섬유강화 폴리머 라미네이트의 확률적 손상해석 모델

정 숭 우
기계항공공학부
서울대학교 대학원

섬유강화 폴리머 라미네이트 복합재료는 고 강도, 질량대비 높은 강성과 같은 장점으로 인해서 많이 사용된다. 이러한 많은 장점에도 FRP는 기지의 강도에 의한 약점을 가지고 있다. 본 논문에서는 섬유강화 폴리머 라미네이트의 확률적 손상해석 모델이 제안하였다. 손상 메커니즘은 라미나 내부의 섬유와 기지의 손상에 관하여 진행하였다. 현재의 결정론적 손상 예측 시뮬레이션 모델은 실험을 통한 결과와의 상관관계가 좋지 않다. 따라서 본 논문에서는 재료 구성물질의 물리적 불확실성을 고려하였다. 이방성 손상 모델은 각 레이어의 손상 시작 및 이후의 손상에 관하여 사용되었다. 각 층의 강도 및 파단 에너지는 Karhunen-Loeve 방법을 통해 공간적으로 변화화하는 무작위 분포로 모델링 되었다. 확률적 손상 시뮬레이션 모델의 설명을 위하여 3차원 라미네이트 구조 유한요소 모델에 적용되었다.

Keywords : 확률적 시뮬레이션, 점진적 손상 해석, 섬유강화 복합재료,
강성, 파단에너지

Student Number : 2017-25727